DIGITAL SUN SENSOR DESIGN FOR NANOSATELLITE APPLICATIONS

KONSTANTIN BOLSHAKOV

A THESIS SUBMITTED TO THE FACULTY OF GRADUATE STUDIES
IN PARTIAL FULFILMENT OF THE REQUIREMENTS
FOR THE DEGREE OF
MASTER OF APPLIED SCIENCE

GRADUATE PROGRAM IN ELECTRICAL ENGINEERING AND COMPUTER SCIENCE
YORK UNIVERSITY
TORONTO, ONTARIO

JANUARY 2020

Abstract

In this research a novel, semi-custom design of a Sun sensor, based on the orthogonal photodiode array design approach, applicable for nanosatellites and other small spacecraft is proposed. A common and well-known strategy of application of a geometrical aperture mask on the light detectors is improved upon and utilised in a non-conventional fashion in the design presented in this thesis. The main characteristic of this design, that is investigated in this work, is the inclusion of a chirped pattern of slits, while using a digital readout of the photodiode arrays. This pattern is expected to allow greater angle detection accuracy while digital photodiode readout decreases complexity and power consumption. The array based design approach is chosen due to lower power requirements, mass savings and simpler readout interface and signal processing in comparison to the matrix based approach. The Sun sensor design presented maximises the accuracy, while keeping the cost, development and implementation time and complexity to minimum. The design will be demonstrated on DESCENT mission CubeSat as a part of the Moth-Eye Anti-Reflective solar cell coating payload. The characterisation of the non-calibrated manufactured part shows that the sensor is capable of 1 degree accuracy, which is expected to improve to under 0.5 degrees with calibration and sensor data processing.

Acknowledgements

First of all, I would like to thank my supervisor, Prof. Regina Lee, for her initial and continuous support and guidance in this research and the academic world in general. This project would have never even been started without her, not to mention the many times her encouragement and reassurance kept me going.

Secondly, I would like to offer my gratitude to the undergraduate students from York University Nicholas Zonta and Fuat Diriker for the great deal of help that they provided while working on the two CubeSat missions. Nicholas has done a lot of supporting work on hardware, such as PCB layout and engineering drawings of the sensor mask, Fuat has done a lot of software work, such as debugging communication interfaces and analyzing raw data for both missions. Thank you for the hard and smart work, for your patience and understanding, for the many things that made this research complete, it would not have been possible without you.

And a special thanks to an undergraduate Research Assistant Daniel Gaine, who volunteered at Prof. Regina Lee's lab and provided great help in the sensor characterisation.

Thank you to all my lab mates: Kajendra Seevananthan, Siddharth Dave, Ryan Clark, Samuel Clemens, Akash Chauhan, Vidushi Jain, Thomas Young, Breannon Lewis, Chitiiran Krishna Murthy for being amazingly supportive, willing to help and provide an objective view on many things.

A big thank you to Dr. Hugh Podmore, who was Prof. Lee's PhD student at the time of my start. His help, inspiration and ideas drove me into this project, and he was willing to help with important conceptual understanding despite his own busy schedule.

Thanks to my friends Evgeniy Shirokov, Kartikeya Bhargava and Raul Palomo as well as my wife Veronika Savina, who provided much needed critical views and moral support.

Lastly, thank you to my parents Galina and Dmitriy Bolshakov for their support in most critical times.

Thank you to all my lab mates: Kajendra Seevananthan, Siddharth Dave, Ryan Clark, Samuel Clemens, Akash Chauhan, Vidushi Jain, Thomas Young, Breannon Lewis, Chitiiran Krishna Murthy for being amazingly supportive, willing to help and provide an objective view on many things.

Table of Contents

List of Tables

List of Figures

"In theory, there is no difference between theory and practice, while in practice there is."

– unknown, 1881 - 1882

Chapter 1

Introduction

A general trend in technology for more than a decade has been miniaturisation: designing and manufacturing increasingly smaller electronic, mechanical and optical components, hence promoting the miniaturisation of various systems containing those components [1]. Motivations behind miniaturisation differ by the industry and application, but common reasons are related to desired improvements in power consumption, performance, reliability and cost [2, 3]. For example, decreasing the size of transistors in nanofabrication leads to higher switching speeds and lower power consumption in CPUs. This also applies to Space industry, namely satellites. Miniaturisation of satellites, first and foremost, decreases the cost of launch due to decreased mass, which is one of the major entry barriers to space for small countries, smaller organisations and research institutions.

Small satellites are defined as satellites of less than 500kg mass, and can be classified into the following categories: mini (100kg to 500kg mass), micro (10kg to 100kg), nano (1kg to 10kg), pico (0.1kg to 1kg) and femto (less than 100g) [4]. Nanosatellites are increasingly popular for and increasingly capable of fulfilling real missions and new technology demonstrations. More than 1000 Nanosatellites were launched in the last decade, and the number of launches is increasing every year [5]. Nanosatellite popularity has led to development and acceptance

of a standard called CubeSat. The standard defines a unified form factor of nanosatellites, which is 10cm by 10cm by 10cm cube of 1kg to 1.3kg mass referred to as "Unit" or "U". A CubeSat commonly consists of integer multiple of CubeSat Units with most common sizes being 1U, 2U, 3U and 6U [5, 6].

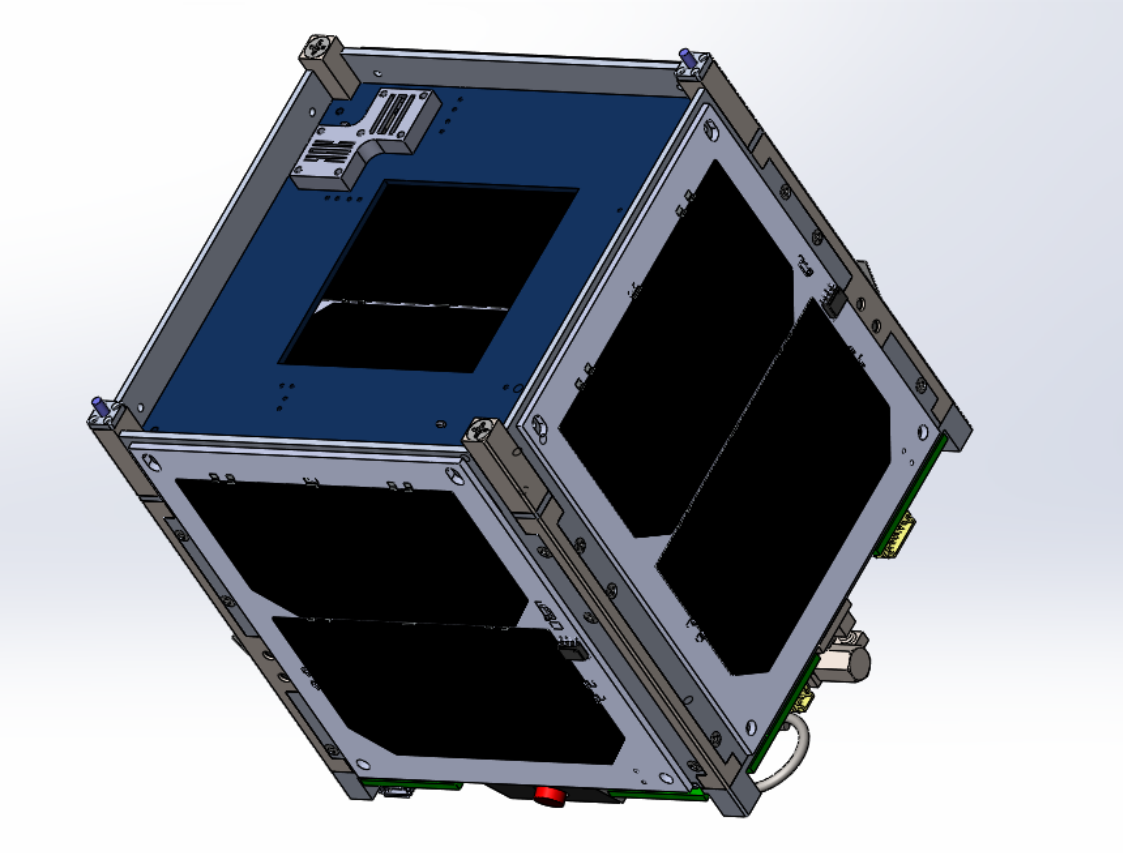

Figure 1.1: 1U CubeSat, one of the two Units of DESCENT mission CubeSat, Mother satellite, with the top side featuring a prototype of the proposed Sun Sensor design.

Source: DESCENT mission design documentation.

The acceptance of the CubeSat standard by the industry has in turn led to availability of standard components such as chassis, On-Board Computers (OBCs), sensors and actuators, as well as "bare-bone" CubeSat development kits [7]. Despite the availability of standard Commercial Off-The-Shelf (COTS) components, certain CubeSat missions require custom or customisable parts for mission objectives, most common of which are payloads and sensors. Additionally, CubeSat missions have low budgets, which means that the components also have to be low cost [8, 9].

1.1 Motivations

One of the integral components of a nanosatellite is a Sun Sensor. It is often used as a part of Attitude Determination and Control System (ADCS) as well as, although less common, a part of a payload system where the orientation of the Sun with respect to the satellite is important for the payload operation. A Sun Sensor is an optoelectronic device, often based on photodiodes, that requires surface area of the satellite in order to expose the required part to the Sun. The main source of power generation for Nanosatellites are solar cells that in most cases are body mounted, as opposed to deployable solar arrays, which are more complex to implement and pertain a high risk of deployment failure [10, 11]. Having low volume, and consequently low surface area, CubeSat designs often maximise the solar cell coverage, which leads to trade-offs with optical sensors. There are several commercially available Sun Sensors, most of which are expensive, large in size or require substantial amount of power to operate. Table 1.1 below compares the existing COTS Sun Sensors potentially suitable for Nanosatellite applications as well as the proposed Sun Sensor, the proposed design metrics are discussed in Chapters 3 and 4.

Table 1.1: Commercially Available Sun Sensors Comparison

Model	**NCSS-SA05**	**NFSS-411**	**BiSon64-ET**	**nanoSSOC-A60**	**nanoSSOC-D60**	**NSS CubeSat Sensor**	**Proposed**
Kind (Analog/Digital)	Analog	Digital	Analog	Analog	Digital	Analog	Digital
Cost (USD)	$12000	$12000	$9630	$2500	$4100	$3300	$1500
Field of View (degree)	114	140	116	120	120	114	114
Accuracy (degree)	0.5	0.1	0.5	0.5	0.5	0.5	0.5
Power supply Voltage	5V	5V	10V	3.3V	3.3V	5V	3.3V
Power (average)	50 mW	37.5 mW	N/A	6.6. mW	69.3 mW	33 mW	N/A
Mass (g)	5	35	24	3.7	6.2	5	4
Temperature range	-25 to 70	-25 to 70	-125 to 125	-30 to 85	-30 to 85	-25 to 50	-40 to 125
Random vibration rating	20g	16.3g	41.4g	14.1g	14.1g	N/A	N/A
Size (mm)	33 x 11 x 6	34 x 32 x 20	49 x 49 x 9.2	27.4 x 14 x 5.9	43 x 14 x 5.9	33 x 11 x 6	23 x 23 x 4.5
Source	[12, 13]	[12, 13]	[14]	[15]	[16]	[17]	This work

Attitude Determination and Control System (ADCS), as the name suggests, is a subsystem of a satellite that determines the attitude (orientation) of the satellite through sensors and controls the satellite orientation through actuators [18]. In most Nanosatellite missions the main function of ADCS is to damp the rotation of the satellite (sometimes called detumbling), fewer missions employ their ADCS for instrument pointing and even fewer for solar cell pointing and ground station tracking due to low pointing accuracy and implementation difficulties [10].

All of the commercially available products are targeted at Attitude Determination usage. Depending on the mission objective, the requirements, such as power budget or sensor interface, will be different and COTS sensors may not be suitable for integration in a payload. We propose a novel low-cost Sun Sensor design, based on orthogonal photodiode arrays, applicable for nanosatellites with high accuracy, low cost and straightforward implementation. The proposed sensor is targeted to be suitable for custom payload integration as well as Attitude Determination Systems.

1.2 Context of the Study

The Sun Sensor presented in this thesis will be demonstrated as a part of two CubeSat payloads integrated into DESCENT mission and Manitoba Sat1 mission. In this section, we provide an overview of the missions for context. More details on DESCENT mission can be found in [19, 20]; more details on ManitobaSat-1 mission can be found in [21].

1.2.1 DESCENT Mission

DESCENT CubeSat mission is aimed to demonstrate an ability of a satellite to deorbit using electrodynamic tether. DESCENT consists of two 1U CubeSat units, held together by a tensioned wire. During deployment, the wire will be cut, separating the two cubes and revealing the 100-meter electrodynamic tether. The tether is designed to collect electrons from the surrounding plasma, while the Spindt array attached to one of the ends of the tether will eject electrons back into the plasma. This will generate Lorentz force that will be the primary deorbiting force. All the mission critical hardware is housed in the satellite with the Spindt array, leaving enough room for additional payloads in the other. [19, 20]

1.2.2 Solar cell Anti-Reflection coating demonstration

The secondary payload on DESCENT satellite is based on the anti-reflective coating of solar cell coverglass as a means to increase the solar cell efficiency. Sub-Wavelength Anti-Reflection Surface (SWAS), also know as SWAR (Sub-Wavelength Anti-Reflection), technology consists of a 2-dimensional array of cones, rods or other spikes spaced in periodic intervals over the surface of the glass. The structures approximate diffraction grating spread evenly across the optical surface and promote absorption of light through the reduction of reflection at the interface of two media [22]. The periodic distance between the structures has to be less than the wavelengths of incident light. SWAS coverglasses have been shown to demonstrate significant anti-reflective effects across wide spectrum of light and wide angles of incidence [22]. To demonstrate this newly developed technology, a stand-alone payload was designed and incorporated in the DESCENT CubeSat as a secondary payload. The high-level architecture of the payload system is shown in Figure 1.2 below. The standalone unit is a 10 x 10 cm custom designed Printed Circuit Board (PCB) with 4 pairs of solar cells, each of which is adhered to a different SWAS coverglass or a regular (non-SWAS) glass for control. Additionally, there are electronic components for in-situ power monitoring of the solar cells, temperature

sensor and a prototype of the proposed Sun Sensor design. The Sun Sensor is included in the payload system to provide a reference of the direction of the Sun vector, which is a required component for evaluating the performance of the SWAS-enhanced solar cells. The solar cells with the antireflection coating are expected to generate more power than the solar cells with regular protective coating at high (above 50°) incidence angle of light, and a Sun Sensor is the tool capable of delivering the angle of incidence to the system. Additionally, having the Sun Sensor mounted on the same payload PCB makes it easier to process the Sun angle data, since it is in the same reference frame.

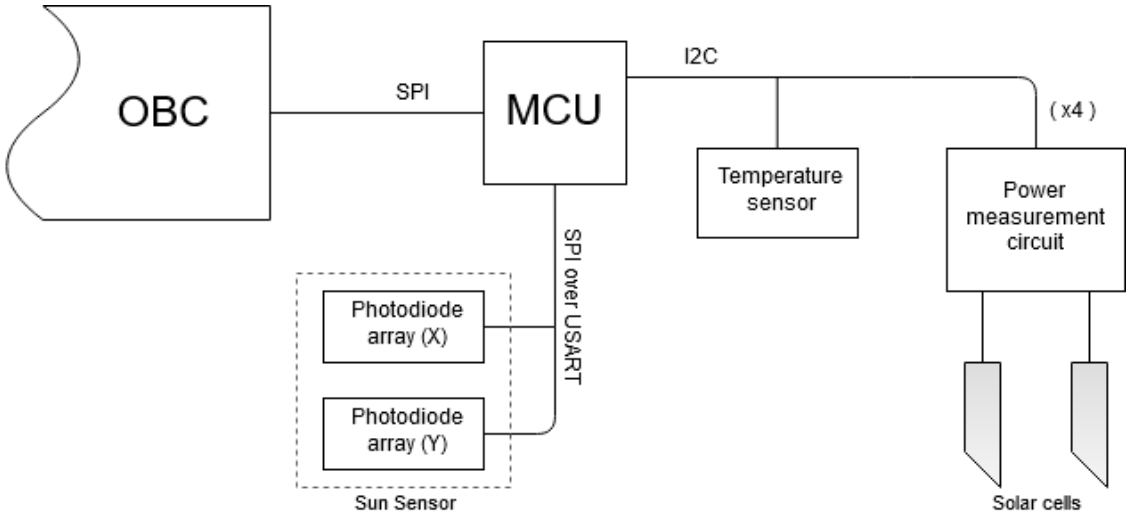

Figure 1.2: High level architecture of the Solar cell antireflection coating payload

1.2.3 ManitobaSat-1 Mission

ManitobaSat-1 project's main mission objective is to investigate how space weather affects asteroids and the Moon through exposing and observing various materials, such as asteroids, to space environment in the Low Earth Orbit [21]. The materials will be exposed to the Sun at different incident angles, which will need to be recorded, and pictures will be taken of the samples periodically [23]. Hence the need for a Sun Sensor in payload context arises. At the time of this writing the project is in early design phase, and few details have been finalised.

1.3 Contribution

Driven by increasing popularity of nanosatellite use for research and commercial purposes, there is a need for high accuracy attitude sensors that satisfy strict weight and size requirements. In particular, Sun Sensor solutions that are commercially available at the moment are too big for a nanosatellite and/or expensive. The application of a geometrical aperture mask on the light detectors of the sensor is a well known and common design strategy for digital Sun Sensors. This strategy is improved upon and utilised in a non-conventional fashion in the design described in this thesis. This design can be implemented in a semi-custom approach, using an off-the-shelf component for the light detector and a custom aperture mask. This would save development time compared to a fully custom solution and would be more cost-effective compared to commercially available units.

A digital Sun Sensor was designed, implemented and characterised. The sensor uses photodiode array based design approach with novel, chirped cosine based, pattern of slits on the aperture mask. The proposed design is flexible and can be used for attitude determination as well as payload support. This Sun Sensor design and demonstration will potentially benefit many small spacecraft projects in research and in the industry. The outcome will contribute to continuous effort in enhancement of small satellite design and development of advanced, low-cost, flexible spacecraft for space-based scientific research as well as the commercial missions. The work presented in this thesis delivers another candidate to space-qualified products of Canadian space industry through flight heritage on two CubeSat missions.

1.4 Overview of the Thesis

This thesis is composed of five chapters. Chapter 1 introduces the Sun Sensor as a part of attitude determination systems used in nanosatellites and presents the main motivations and the need for this work as well as the context of the sensor demonstration in CubeSat payloads. Chapter 2 compares the Sun Sensor to other common attitude determination sensor used in nanosatellites, outlines the positive and negative aspects of including a Sun Sensor in a payload and states the research objectives of this work including rationale. Chapter 3 provides a comparison of existing Sun Sensor design approaches and describes the proposed Sun Sensor design in detail. Chapter 3 also describes the necessary design alterations taken due to various limitations imposed on the projects and design aspects related to the integration of the sensor into two different CubeSat payloads. Chapter 4 describes the laboratory setup used for the characterisation of the manufactured Sun Sensor part and presents the results of characterisation along with the meaning of observations. Chapter 5 concludes the thesis, summarising the contribution of this work, discusses future work and possible improvements.

Chapter 2

Background

2.1 Attitude Sensor comparison

In this thesis we focus on the Sun Sensor and will briefly describe other popular attitude sensors that are used in CubeSat missions [10, 24].

2.1.1 Star tracker

Star trackers are based on a Charge-Coupled Device (CCD) or Complementary Metal Oxide Semiconductor (CMOS) matrix photo-detectors similar or sometimes identical to the ones used in digital cameras. The orientation of the satellite is calculated from the captured images of the stars by comparing them to a star map database [25]. Star trackers are very high precision attitude sensors, capable of achieving down to 1 arcsecond accuracy. However they are expensive, complex, heavy, require substantial amounts of power and memory and cannot be used in presence of sunlight [24].

2.1.2 Magnetometer

Magnetometers consist of three orthogonal magnetic sensors that measure the magnetic field of the Earth, which is then compared to a model of the Earth's magnetic field, such as International Geomagnetic Reference Field (IGRF), in a Kalman filter implementation [24]. Magnetometer is a very popular attitude sensor for small satellites, due to the pronounced strength of the magnetic field in the Low Earth Orbit (LEO), which is the orbit of choice for many small spacecrafts [24]. The major advantages of using magnetometers for CubeSats are their small size and low power consumption as well as reasonably straightforward implementation [26]. The downsides of using magnetometers are the requirement for precise and sometimes in-flight calibration as well as the necessity of dealing with the magnetic noise produced by the spacecraft electronics [26].

2.1.3 Gyroscope

Gyroscopes measure angular rotation rate of a satellite, which has to be integrated to obtain disposition; traditional gyroscopes with spinning wheels are too bulky and heavy for small satellites, so various Microelectromechanical Systems (MEMS) approach devices are more popular for satellites [24, 27]. MEMS gyroscopes are small in size and require little power; however the drift caused by integration poses the need for calibration and the inertial nature of the sensor makes it most effective in combination with other sensors [24, 27].

2.1.4 Sun Sensor

Sun Sensors detect the orientation of light in two axes, hence inferring the pointing direction toward the Sun [28]. Various analogue and digital Sun Sensor designs exist (covered in more detail in section 3.1) all of which involve some form of photo detector and most of them a supporting geometric structure placed over the detector [28]. The accuracy of Sun Sensors ranges from 2.5° or worse using solar cell current measurement [29] to 0.1° or better with

the use of dedicated hardware and complex processing algorithms [28]. Similar to many other sensors, Sun Sensor accuracy can be a direct trade-off with it's size, weight and power consumption; what makes a Sun Sensor unique is the variety of design approaches to the solution of the problem of the Sun tracking (discussed in more detail in section 3.1), many of which are simple and reliable. This makes Sun Sensor one of the best candidates for customisation and integration into projects with demanding constraints.

2.2 Sun Sensor in payload support

Sun Sensor is a common attitude determination sensor, used by small and large satellites alike in the ADCS systems. The Sun Sensor proposed in this thesis will be demonstrated on two CubeSat projects as a payload support sensor rather attitude control system. This poses more strict requirements on the sensor, forcing the design to be more self-contained. Since the sensor has to be integrated with other payload components, it is desirable to have a customisable design with simple electrical interface.

2.2.1 Positive aspects for payload integration

Sun Sensors can be integrated into almost any payload due to the variety of available designs, some of which are small, light and have minimal area footprint. Sun Sensor is self-sufficient, does not depend on data from any other sensors and does not require in-flight calibration. Many designs are low power, which is always desirable for a satellite, and can be switched off when readings are not required for further power efficiency improvement. Most spacecraft payloads have a Micro-Controller Unit (MCU) or a Micro-Processor Unit (MPU) as the central processor that a Sun Sensor can be directly connected to; most of the MCUs and MPUs have built-in Analogue to Digital Converters (ADCs), thus both analogue and digital designs can be integrated with minimal additional resources and components. Lastly, when

mounted in the coordinate system of the payload, the Sun Sensor data requires no frame or coordinate translation and can be directly used with the other payload data.

2.2.2 Challenges and limitations for payload integration

The main limitation of integrating a Sun Sensor in a payload is, of course, the dependence on the Sun. It is therefore only feasible for payloads that operate in the presence of sunlight. Another downside of a Sun Sensor integration is additional computational requirements for on-board Sun direction calculation. This can be alleviated by carrying out the computations on the ground for the payloads that do not require that data as an input. However depending on the design and implementation this approach may lead to another downside, which is data storage requirement. Fortunately, this is less of an issue these days, since flash memory size and cost are very low.

2.2.3 Sun Sensors in satellite payloads

Little can be found about small satellite payloads that integrate a Sun Sensor or are composed of the Sun Sensor alone. With the most common scenario including a Sun Sensor as a payload for technology demonstration of that very sensor or for educational purposes [30]. The practice of hosting secondary and tertiary payloads, that is common for larger spacecraft, is already making its way into small satellites. As such, the DESCENT mission is hosting the Solar cell demonstration payload as secondary payload on the CubeSat [20]. It is entirely possible that in the future the standalone payload integration into small satellite missions will become more common, similar to many other things that were inherited by micro and nanosatellites from their larger precessors.

2.3 Research objectives

There has been significant advancements made in CubeSat industry, allowing low-cost, easy access to technology demonstration, space-based commercial activities and science missions. For the two payloads that are under development, namely the SWAS Anti-Reflection coating demonstration and the ManitobaSat-1 payload, we identified a need for an accurate attitude sensor with low mass, low power, simple reusable interface that can be integrated in a CubeSat mission with little adjustments to the design of the spacecraft.

The best possible sensor solution, potentially exceeding all the requirements, would have been a custom Application-Specific Integrated Circuit (ASIC). A custom ASIC could integrate most of the Sun Sensor components on a single chip, greatly minimise the size of the sensor and reduce the power consumption, which is highly desirable for nanosatellites. Farian et al. present and demonstrate such a sensor in their published works [31, 32]. However the cost of manufacturing a custom ASIC, the time required to design and lay it out were too great for the scope of this project, and are similarly too great for the scopes of most nanosatellite mission projects. Instead, a semi-custom solution is proposed that can be replicated by nanosatellite teams within reasonable time, and is likely to be within many similar projects' budgets. The proposed design is low power, small, cost-effective and provides reasonably high accuracy for Nanosatellite missions; it is discussed in section 3.2.

Chapter 3

Sun Sensor Design

3.1 Existing Sun Sensor Designs

As described in earlier chapters, Sun Sensors detect the orientation of the Sun with respect to a local frame of reference. Most common Sun Sensor designs are composed of a photodetector and a mask directing or partially blocking the light reaching the detector. In this section we present a set of existing Sun Sensor Designs implemented in real products as well as conceptually presented in academic resources.

3.1.1 Photodiode based

The simplest form of a Sun Sensor is the one that omits the aperture mask and relies on the analogue readout of photodiodes. One photodiode is usually placed on each face of the satellite such that the sensor is capable of measuring the incident light intensity along the axis of each face, each measurement is then converted to a component of the Sun vector in the frame of the satellite [33]. This is illustrated in Figure 3.1, where each face of the cube has a small dark rectangular area representing the photodiode with a unit vector normal to the surface representing arbitrarily defined positive direction for the given axis. This

coarse sensing design is common for nano- and smaller-sized satellites due to fairly small area requirement and relatively simple computations involved [33].

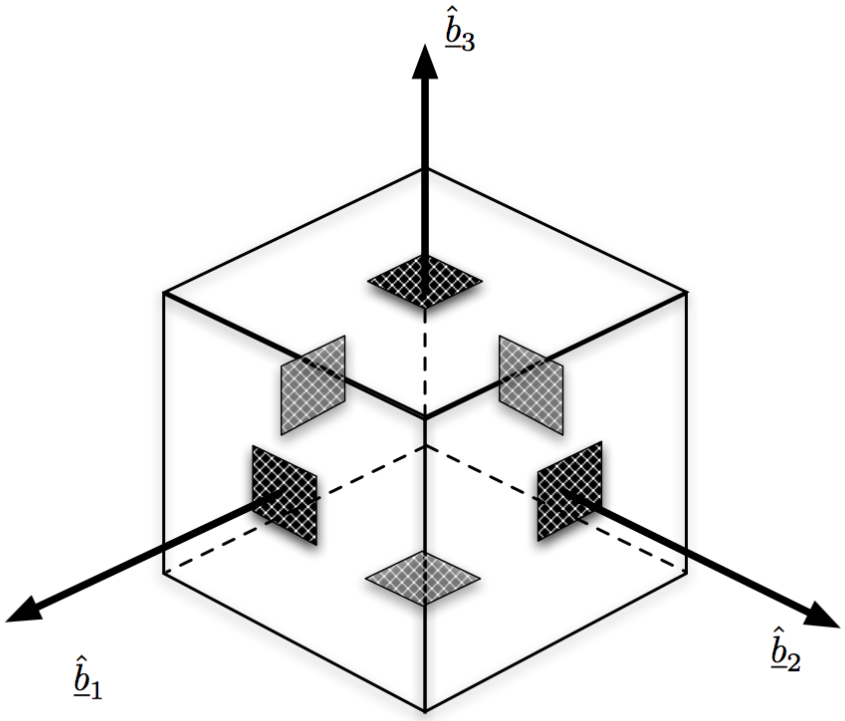

Figure 3.1: Geometry of photodiode based Sun Sensor. One photo-detector is placed on each face of the cube, aligned with the frame of the satellite.

Source: [33]

The advantages of photodiode based design are low cost and low mass due to very few components required as well as minimal surface area occupied on the face of a satellite. Most of the Micro-Controller Units (MCUs) come with at least a few Analogue to Digital Converters (ADCs), which means that the analogue readout from the photodiodes can be converted and processed in the MCU itself, eliminating the need for additional hardware. This design is often implemented in conjunction with other attitude determination sensors, such as magnetometers and gyroscopes, to increase the overall determination accuracy without

violating mass and power budgets [34]. The main disadvantage of this sensor is the heavy processing to accuracy trade-off. With simple signal processing the accuracy is fairly low. Complex processing algorithms can improve the accuracy significantly, but at a cost of computational power and potentially difficult implementation. The design is becoming less common due to development of small inexpensive sensors with higher accuracy.

The field of view of diode based Sun Sensor is theoretically 360 degrees, since the filed of view of each sensor overlaps with the neighbouring ones. The accuracy of this sensor design can range significantly depending on the complexity of the processing and angle range. Allgeier et. al in their analysis report measurement error ranging from 3 to 17 degrees [33].

3.1.2 Solar panel current based

An alternative to dedicated photodiodes for light intensity detection is to use solar panels, that are commonly found on even the smallest satellites. The geometry of this design is very similar to the photodiode based one. Each face of the satellite has one or more solar cells mounted. Using a trigonometric approach, the relationship between the current outputs and the incident angle of light can be established [35].

The advantages of solar panel current based design are similar to the photodiode based one: low cost and low mass due to even fewer additional components required: usually none or, in case of one face of the satellite not having any solar cells, one photodiode to complete the coverage. It is therefore often implemented on small missions that do not allow additional part due to mass or other budget restrictions and projects seeking to reduce weight and cost [35]. The main disadvantages of the solar panel sensor design are also low accuracy and complex processing, since this method relies on processing small analogue values of low precision readout circuits.

The field of view is the same as the photodiode based design's (360 degrees), since the filed of view of each solar cell face overlaps with the neighbouring ones. The accuracy of solar

panel based sensor, similar to photodiode based design, can range greatly with factors such as Analogue to Digital Conversion (ADC) precision, processing complexity and sensor model [35, 36]. In their unique solar cell based analogue Sun Sensor design Kocian et. al report the error of angle detection as approximately ± 3 degrees [30].

3.1.3 Quadrant based

The traditional design of a Sun Sensor is based on a 4-segment photo-detector arranged in a 2 by 2 matrix with an aperture mask that has a single slit in the middle. The light passes through the slit resulting in a single spot that covers all 4 segments with varying intensity, which is used to infer the Sun angle [37]. The operational principle is illustrated in Figure 3.2 below. The aperture mask is place on top of the detector and the height of the mask from the surface of the detector is denoted as h. The mask has a single square aperture, and the length of the side of the square is denoted by the letter L, while the thickness of the mask is denoted by letter a. The sunlight comes at an arbitrary angle that is split into two components denoted as α and β. The quadrant detector composed of four segments labelled as S_1 through S_4 receives the image of the aperture distributed between the four quadrants. The light intensity detected by each quadrant is then read and processed to infer the angled α and β.

The main advantage of the quadrant design is a relatively simple geometry and low cost, which comes from the simplicity of components. The main disadvantage of the quadrant design is low accuracy at wide field of view, albeit it is higher than the previously described designs.

The accuracy of the quadrant design and other mask-based designs increases with the distance between the detector and the mask. This same distance, also commonly referred to as height, is inversely proportional to the field of view. It is therefore understood that it is difficult to realise both high accuracy and wide field of view, which is expressed and

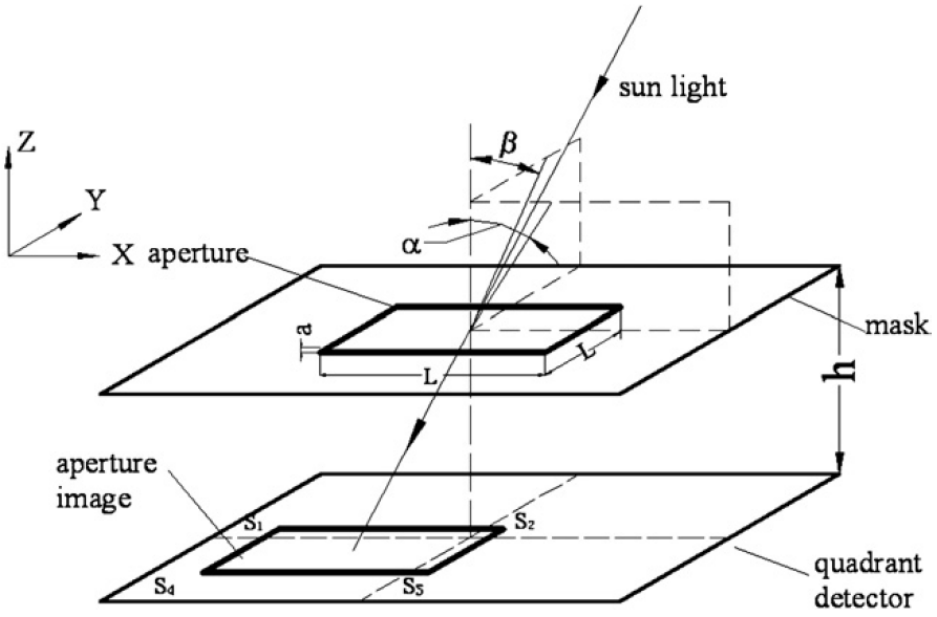

Figure 3.2: Operational principle of the traditional 4-quadrant analogue Sun Sensor. An aperture mask with a single hole in the centre is placed on top of the quadrant detector.

Source: [38]

addressed by Chen and Feng in [38]. They present a measuring principle for analogue Sun Sensors and apply it to a prototype of a sensor based on the quadrant design. The accuracy they report from their tests is 0.2 degrees with ±62 degrees field of view [38].

3.1.4 Matrix based

An extension of quadrant based approach is Matrix-based design, where the photodetector part consists of a matrix of photodiodes, the size of each row is typically in hundreds of pixels. An active pixels sensor (APS) such as CMOS or CCD, used as a light detector, allows for multitude of options for the design of the aperture mask. Those include simple slit, multiple slits, a cross, 'L' shaped and others. A simple diagram depicting the multi-aperture mask above an APS detector is presented in Figure 3.3. A plot of the sampled pixel readings in

the area of a single aperture is presented in Figure 3.4.

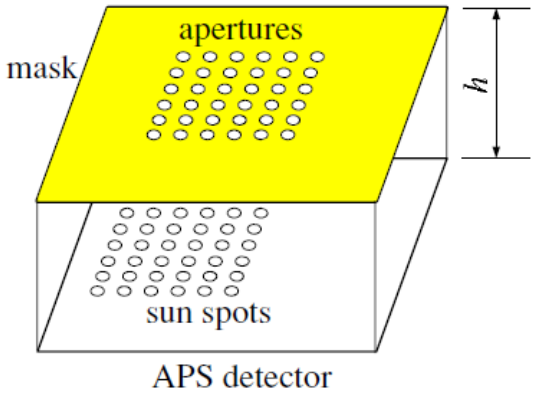

Figure 3.3: Matrix detector with multiple same-sized apertures on the mask.

Source: [39]

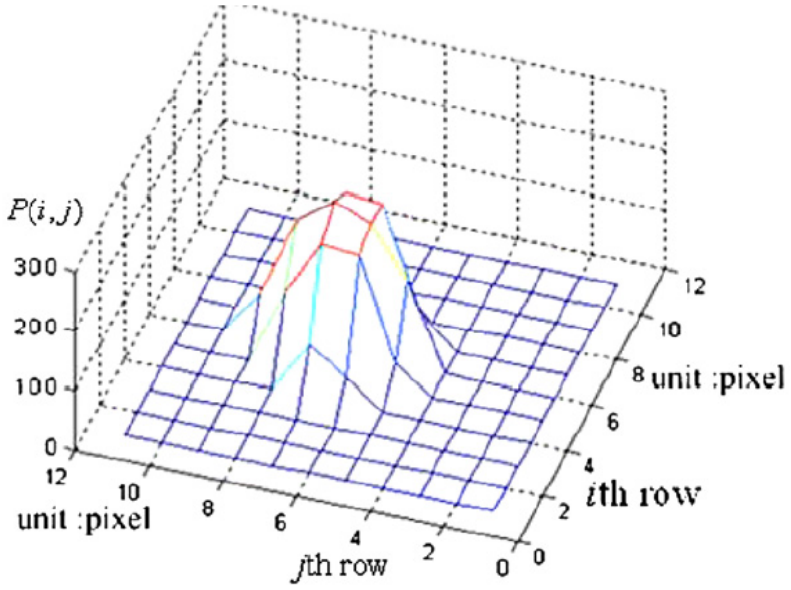

Figure 3.4: Visualisation of data captured by a region of pixels, illustrating a single aperture detection.

Source: [39]

The main advantage of the photodiode matrix or image-sensor based design is its potential for high accuracy, which depends on the design of the aperture mask and signal processing. Another advantage worth noting is the flexibility and variety of possible aperture mask designs.

The main disadvantage of the image-sensor based design is the complexity of the implementation: APS image sensors often employ sophisticated digital interfaces that require hardware converters or specialised controllers for processing, or alternatively the analogue value of each of matrix photodiode may be read one pixel at a time, which increases the complexity of the processing of the data.

The accuracy of photodiode matrix based design is generally the highest of the designs discussed in this chapter. It comes at the cost of fairly large surface area required for the sensor, mask and often additional converters or processing circuits. Additionally, to achieve this accuracy, computationally intensive image processing algorithms are employed. Xing et al. in 2008 proposed a technique for improved accuracy of their APS based Sun Sensor. They report accuracy of 0.0059 degrees at ± 64 degrees range [39].

3.1.5 Array based

A simplified version of a matrix based design is a dual-array configuration. The two photodiode arrays are arranged perpendicular to one another and aligned with the frame of the spacecraft. This design removes the majority of the pixels from the matrix, leaving only one row and one column, resulting in a similar configuration that is capable of sensing two-dimensional orientation. Each of the two arrays corresponds to an axis. Similar to the matrix based, this design approach allows the freedom of employing various aperture mask configurations, such as single slit per array, 'L' shaped and multi-slit per array.

The main advantage of this design is the potential for high accuracy, similar to the matrix approach, while at the same time minimising the number of pixels used for sensing,

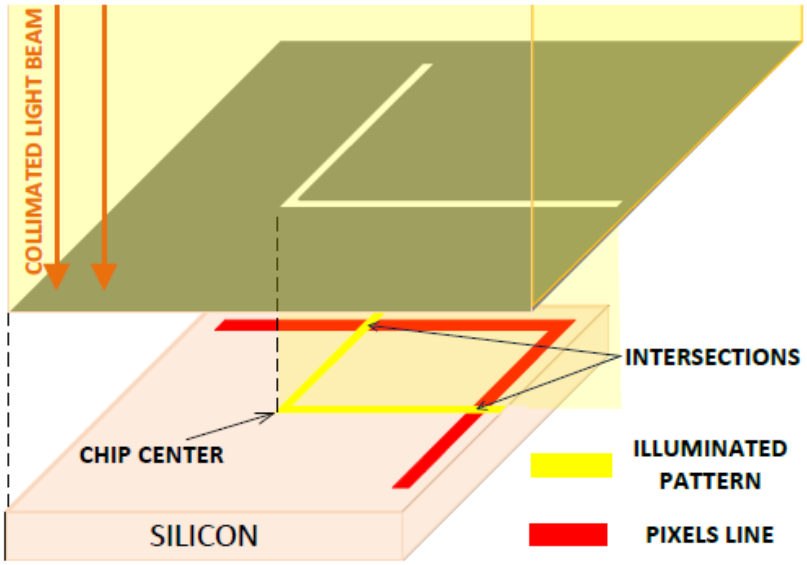

Figure 3.5: Operational principle of the traditional 4-quadrant analogue Sun Sensor. An aperture mask with a single hole in the centre is placed on top of the quadrant detector.

Source: [32]

hence reducing the power consumption and eliminating the need for complex interfaces or sophisticated data processing.

The main disadvantage of the array based design is the surface area required for implementation. While it is a simplification of the matrix based design and the number of pixels is reduced significantly, the surface area reduction is minimal due to the need of the mask mounting.

As mentioned before, the accuracy of the mask based designs, including the array based design, increases with the distance between the detector and the mask, while the field of view decreases with the same distance. Farian et al. in their work on an design of an on-chip array based Sun Sensor with an 'L' shaped mask report the accuracy of 0.42 degrees at ± 60 degrees field of view based on the characterisation of the real manufactured part [32].

3.1.6 Summary

The following table summarises the comparison of the presented Sun Sensor design approaches. It is Concluded that the most balanced overall is the array based design, where the accuracy can potentially be increased by optimising design parameters presented later in this chapter.

Table 3.1: Common Sun Sensor design approach comparison

	Diode	**Solar panel**	**Quadrant**	**Matrix**	**Array**
Field of view (degrees)	360	360	120	120	120
Best accuracy (degrees)	3	3	0.2	$<$0.01	0.42
Additional footprint	Small	Very small	Medium	Large	Large
Additional mass	Small	Very small	Small	Medium	Small
Implementation complexity	Complex	Complex	Moderate	Very complex	Moderate

3.2 Proposed Sun Sensor Design

The proposed Sun Sensor design that we have developed for DESCENT and Manitoba Sat-1 missions is based on the Array design approach. It consists of 2 orthogonal photodiode arrays, each with integrated readout circuits, and an aperture mask with multiple slits integrated in a custom PCB. The proposed design is a hybrid between fully custom and ready off the shelf solution. The photodetector chips used are commercially available integrated circuits (ICs) with built-in Analog to Digital Converters (ADCs) and Serial Peripheral Interface (SPI) communication protocol. Designing and fabricating an Application-Specific Integrated Circuit (ASIC) is difficult, time consuming and expensive, while resulting in the best possible solution to many problems, including the design of a Sun Sensor. Designing a custom Printed Circuit Board (PCB) to mount the ICs in various packages in custom orientation is less difficult and much more attainable for a variety of projects, including Nanosatellite missions. In this design a custom PCB was designed for the detector ICs, which also incorporated the

mounting holes for a fully custom designed and fabricated aperture mask. The same PCB also housed the electronics for the Sun senor data processing alongside the electronics for the Solar Cell Anti-Reflection payload. In this section we describe each component and design parameters associated with the proposed Sun Sensor design.

3.2.1 Aperture mask

In designing an aperture mask various shapes proposed in the literature were considered. A multi-slit aperture (see Figure 3.6) was selected for several reasons. Multiple slits provide a pattern of light that consists of several lit and shaded areas. When the pattern moves along the array, each boundary between lit and shaded area provides a point of reference, which are the basis of the angle detection. Specifically, in this work, a pattern of slits based on the chirped cosine function was chosen as an innovative approach to multiple slit mask.

The light detectors of the proposed Sun Sensor consist of two photodiode array ICs in orthogonal orientation, which are discussed in more detail in the next subsection. Since the two detectors are identical, the design of the mask was approached in one dimension. The aperture mask is placed directly on top of the photodetector array chip, such that the centre of the pattern is above the centre of the diode array. The height of the mask, h, is defined as the distance between the surface of the photodiodes and the bottom surface of the aperture (see Figure 3.6). The pattern of light that results from the light passing through the mask can be thought of as a means to convert the angle of the light source with respect to the detector to displacement. This conversion is done through a simple trigonometric identity:

$$tan\theta = \frac{d}{h} \tag{3.1}$$

In this equation (3.1) angle θ represents the desired resolution of the sensor, the distance d is the pixel pitch of the photodiode array, leaving the height h as the unknown. In their work on a miniaturised Sun Sensor based on the array design approach Farian et al. designed, and manufactured their own photodetector arrays integrated with the aperture mask in a

single chip [32]. Their chip was manufactured on the AMS 0.35 μm opto-process with 8 μm pixel pitch [31]. Thus it is realistic to assume that 8 μm pixel pitch is easily achievable on a mass produced photodiode array. Following this assumption, the resolution goal for the Sun Sensor was 0.2°, which yields $h = 8\mu m \div tan(0.2°) \approx 2.3mm$.

The same equation is used by Chum and Vojta in their work on a wide angle digital Sun Sensor based on a CCD linear array as the basis of the filed of view analysis [40]. They point out that in their single-slit design the field of view larger than ±45° significantly reduces the resolution of the sensor due to the steep rate of change of the tangent function beyond ±45°. Additionally, taking into consideration that stray light reflected by the photodiodes and the aperture mask increases at higher incidence angles and contributes significantly to the error, their conclusion was that the maximum reasonable field of view for their sensor was ±60°, which is the same as the field of view of higher end commercially available products.

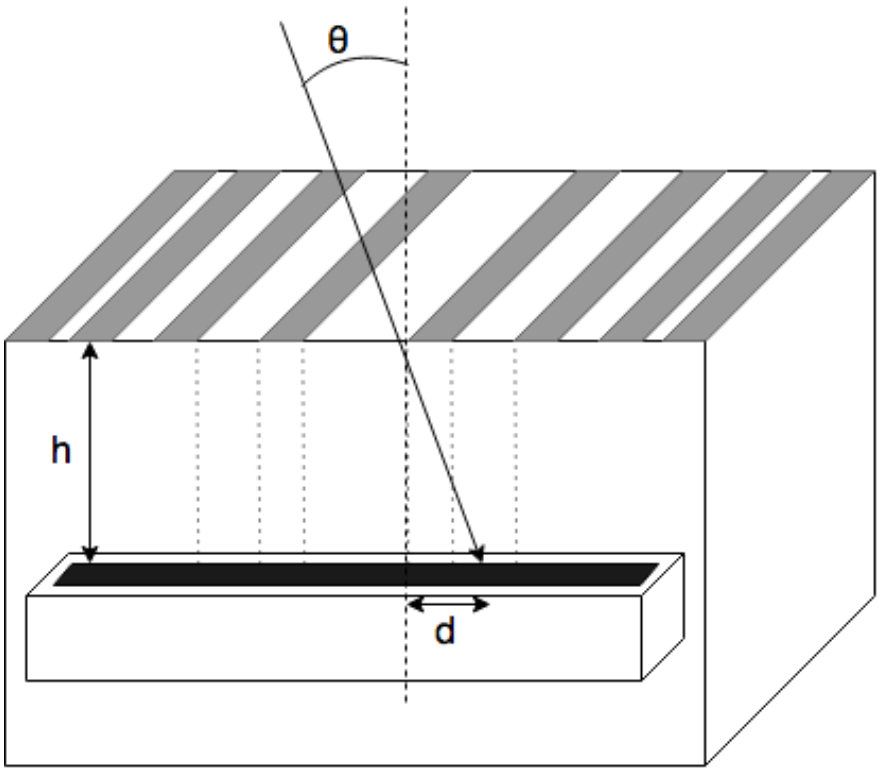

Figure 3.6: Proposed Aperture mask of the Sun Sensor design.

The focus of the proposed design was to maximise the accuracy while keeping the cost, power consumption and implementation difficulty at their minimum. Thus, the most important parameters of the aperture mask were determined to maximise the accuracy. Using those parameters, the field of view was estimated to be $\pm 57^{\circ}$ (Equation 3.2) and is only slightly lower than the best commercially available sensors.

$$\theta_{FOV} = tan^{-1}(\frac{d_{max}}{h}) = tan^{-1}(\frac{3.55mm}{2.3mm}) \approx 57^{\circ} \tag{3.2}$$

In order to validate the established and determine the remaining design parameters a mathematical simulation study was performed using MatLab. Chirped cosine function was taken as a basis for the pattern of the aperture mask. The simulation was performed on a 7-slit mask sensor and a single-slit mask sensor, both generated using a general form of chirped cosine function and is shown in Figure 3.7 and Figure 3.8. The function used to generate the aperture mask patterns is presented in Equation 3.3, where x is the displacement along the length of the detector array in μm and C_{ch} is the chirp coefficient determined empirically together with power a. The coefficient C_O is the offset to centre the cosine pattern on the mask, while keeping the origin at the left edge of the sensor.

$$f(x) = cos\left|\frac{1}{C_{ch}}\frac{\pi}{180^{\circ}}(x - C_O)^a\right| \tag{3.3}$$

The sensor readout was simulated with Gaussian noise superimposed at signal to noise ratio (SNR) of 20 dB to account for noise without considering the sources separately. Two simulated readouts: one at 0 μm and one at 30 μm offset are presented in figures 3.9 and 3.10 for each sensor model.

To ensure that the detector reading corresponds to only one location of the pattern and therefore only one incident angle of light, Root Mean Square (RMS) difference of the true centre of the pattern and every other coordinate was taken for $0\mu m$ and $30\mu m$ offsets. The formula used for the RMS difference calculation for each point x on the pixel array for $0\mu m$ offset is presented in Equation 3.4; x varies within the bounds of the physical size of the detector array and is in μm units, whipe p is the number of pixels, and hence the number of elements in each *reading*. The results for both offsets plotted for each sensor model are presented in Figure 3.11 and Figure 3.12. The plots show a distinct global minimum at the true centre of the pattern, which illustrates that the only ambiguity in the reading is found around that area.

$$f(x) = \sum_{i=1}^{p} \sqrt{(reading_i(0) - reading_i(x))^2} \tag{3.4}$$

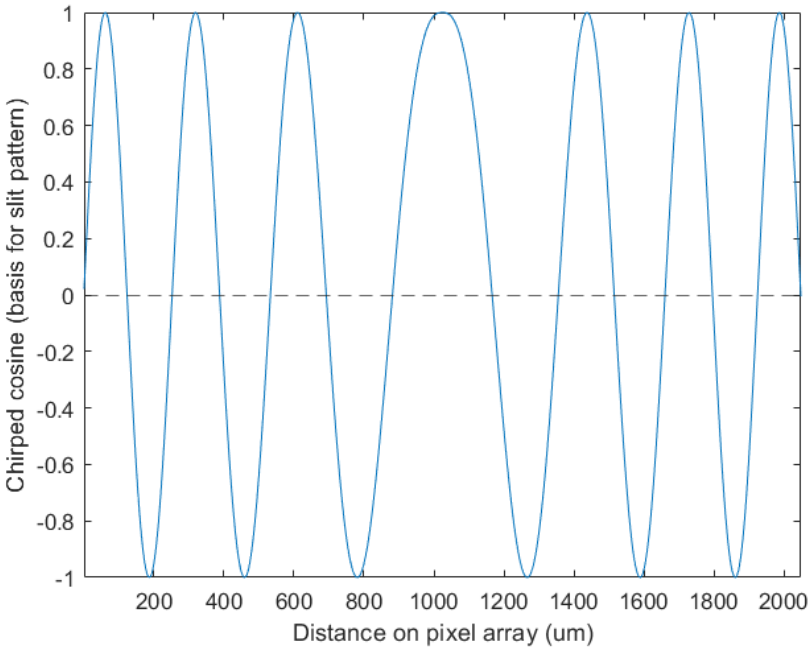

Figure 3.7: Chirped cosine function used as the basis of the slit pattern of aperture mask

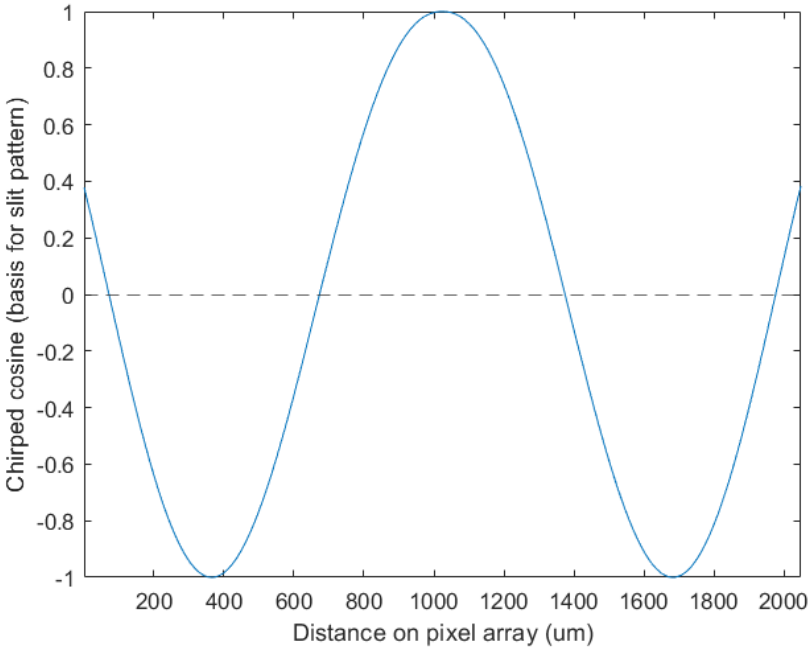

Figure 3.8: Chirped cosine function reduced to single slit pattern of aperture mask

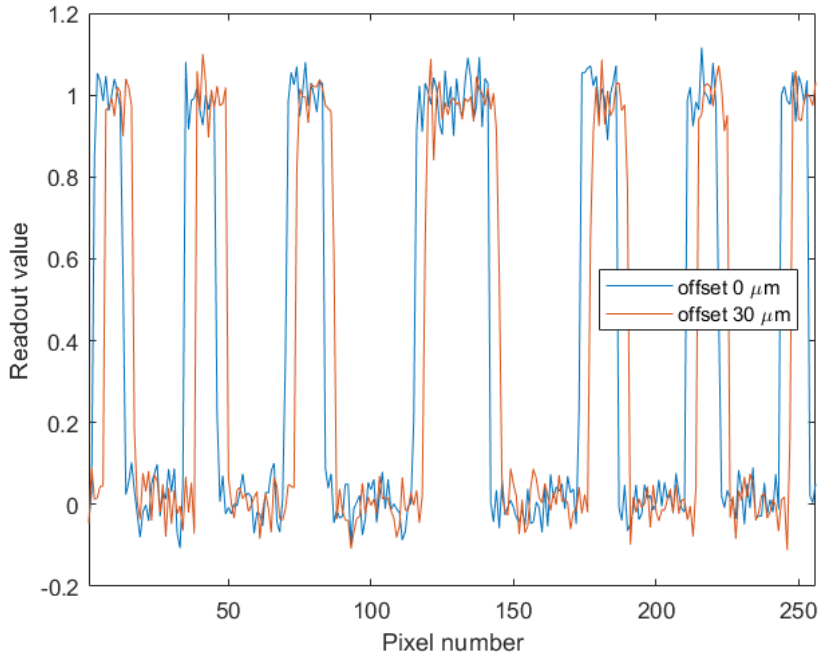

Figure 3.9: Pixel array readouts for chirped light patterns centred at $0\mu m$ and $30\mu m$ offsets

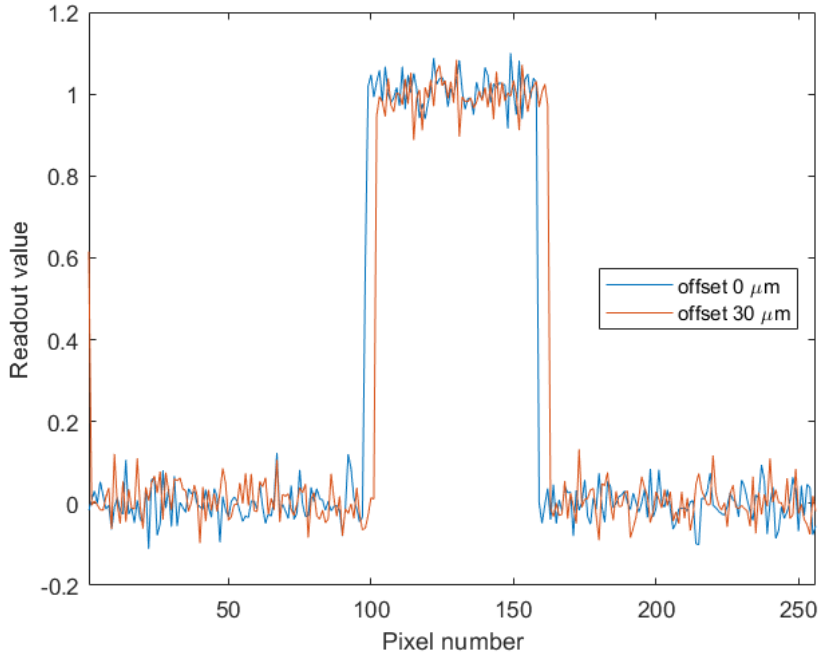

Figure 3.10: Pixel array readouts for single slit patterns centred at $0\mu m$ and $30\mu m$ offsets

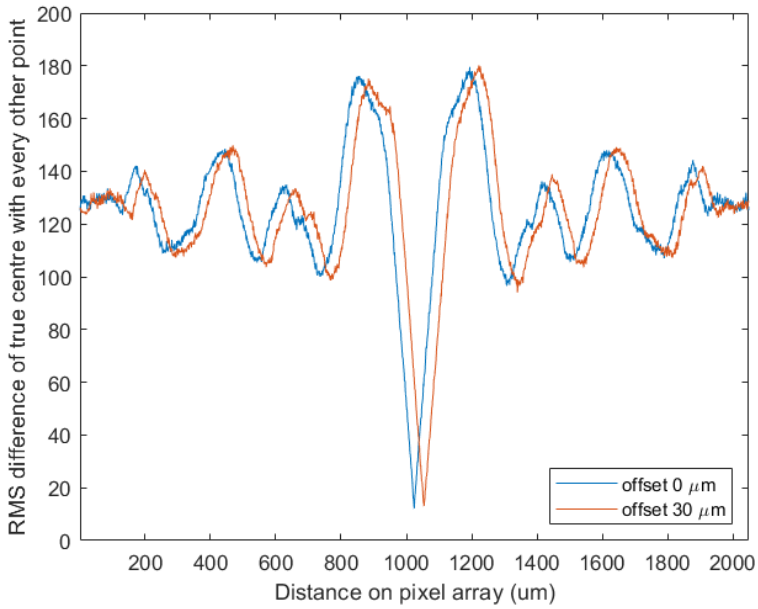

Figure 3.11: RMS difference of true centre of the projected chirped pattern and all other possible locations on the sensor

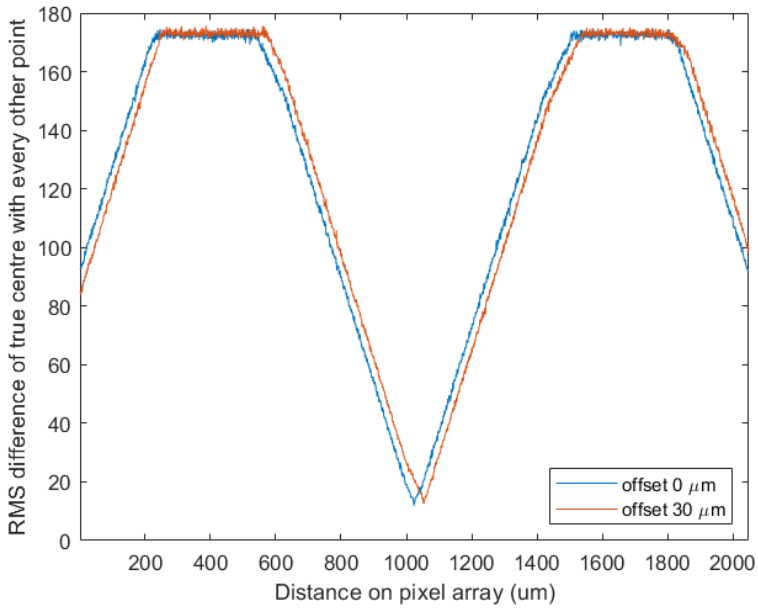

Figure 3.12: RMS difference of true centre of the projected single slit pattern and all other possible locations on the sensor

To illustrate the importance and the need for chirped cosine based pattern, the same simulation was done on the multi-slit pattern with the same slit size of 80 μm. Figure 3.13 depicts a scenario where two independent readings are arranged in such a way that the slits nearly overlap, close to an offset by one full slit. The RMS difference for both of the readings was also calculated and is presented in Figure 3.14. This figure illustrates that the local minima of the RMS plot of a given reading are fairly close to one another, which may introduce ambiguity in determining the angle. The same can be observed when comparing the global minimum point of one reading and the nearest local minimum point of the other reading. The RMS values are very close to one another and could be misinterpreted under certain conditions, such as higher noise levels. Comparing Figure 3.11 and Figure 3.14, it can be seen that the proposed chirped cosine slit pattern provides better noise resilience and better differentiation of individual readings.

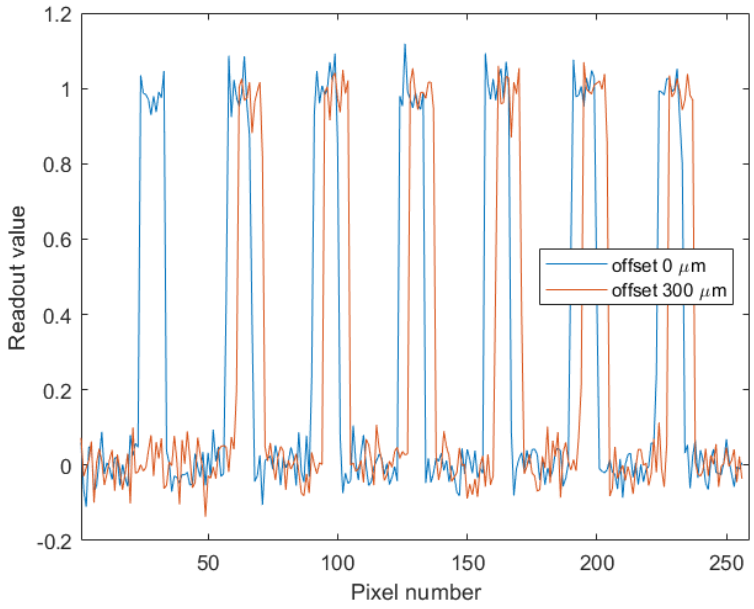

Figure 3.13: Pixel array readouts for same size slit light patterns centred at $0\mu m$ and $300\mu m$ offsets

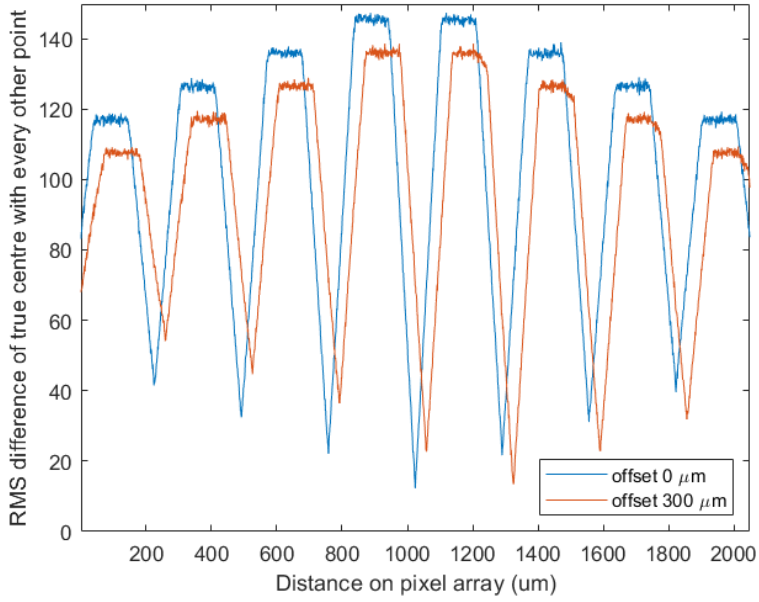

Figure 3.14: RMS difference of true centre of the projected same size multi-slit pattern and all other possible locations on the sensor

$$O_r = \frac{3\sigma}{m} \tag{3.5}$$

To compare the two sensor models a noise equivalent reading offset (O_r) was defined (see Equation 3.5). The RMS difference shown in Figures 3.11 and 3.12 can be approximated by a line immediately left and right of the global minimum. These lines represent the change in error per change in the pattern offset on the detector, hence the rate of change (slope m of the lines) represents the rate of change of the error. Since the noise was modelled by a commonly used Gaussian distribution, a 3σ value was computed by the same MatLab simulation after taking 2048 samples of the noisy measurement of the $0\mu m$ pattern offset; the resulting distributions, including the centre and $\pm 3\sigma$ values, are presented in Figure 3.15 and Figure 3.16. The 3σ values are the characteristics of the noise model, and are very similar for both models as expected: 1.8745 and 1.8464 respectively. The slope m however is the characteristic of the model relating directly to the aperture mask. The slope was calculated by simply taking 2 points from the line to the right of the minimum on the RMS graph. The reading offset values for the chirped mask and the single-slit mask are presented in Equation 3.6 and 3.7 respectively; the units of all values are μm.

$$O_r(chirped) = \frac{1.8745}{1.5913} = 1.1782 \tag{3.6}$$

$$O_r(single) = \frac{1.8464}{0.3371} = 5.4773 \tag{3.7}$$

The calculations show that the offset of the single-slit mask is significantly higher (approximately 5.5 μm) than the reading offset of the chirped mask sensor model (approximately 1.2 μm), which is expected due to multiple slits providing multiple points of reference as well as a chirped pattern providing different, distinguishable slits.

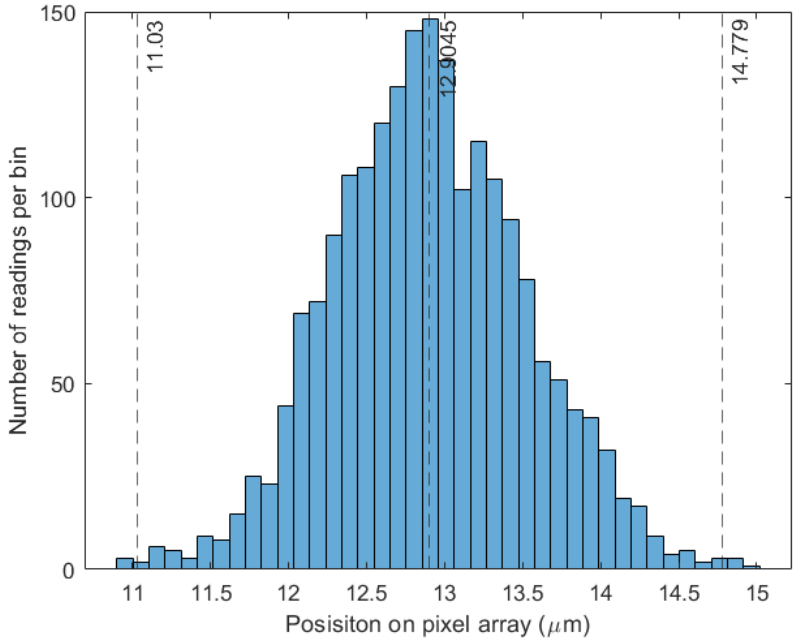

Figure 3.15: Noisy measurement distribution of 2048 points given SNR of 20 dB

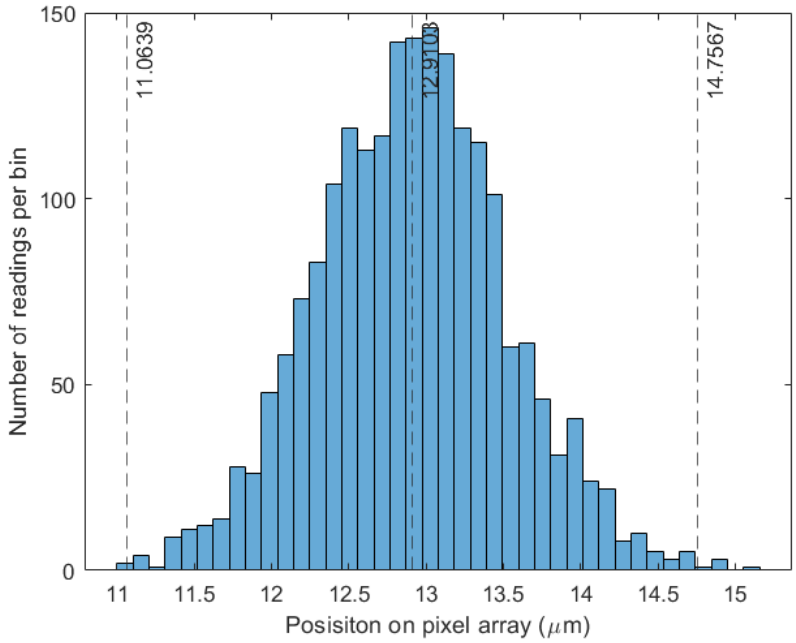

Figure 3.16: Noisy measurement distribution of 2048 points given SNR of 20 dB

3.2.2 Photodetector

A survey of linear image sensors was conducted at the start of the project. Several parameters had to be considered for the design and implementation of the sensor, which are summarised in Table 3.2. A size constraint was imposed by the two missions in which the sensor is to be demonstrated, which is common for nanosatellite missions. Given this constraint, only a limited number of products was considered.

Table 3.2: Available linear array sensors characteristics

	TSL1401	**TSL3301**	**MLX75306**	**TCD1103GFG**
Pixel count	128	102	142	1500
Pixel size (um)	55.5	77	47	5.5
Pixel pitch (um)	63.5	85	50	5.5
Array size (um)	8120	8573	7100	8250
Package size (mm)	9.4x3.0	9.4x3.0	9.93x6.0	15.2x6.0
Sensor type	CMOS	CMOS	CMOS	CCD
Interface	Analogue	Digital	Digital	Analogue
Power	3V	3V	3.3V	3V
Package	CL	CL	SMD	CL
Availability	yes	yes	yes	no
Cost (CAD)	$12.01	$15.22	$20.67	$21

Along with size, the most important parameters considered for the implementation were the package and interface of the IC. The CL package of the TSL sensors poses additional difficulties on prototyping: it requires a custom PCB with custom footprint, which is considerable in time, effort and cost. ICs with analogue output require additional components as well as additional data processing. Moreover, analogue signal lines on a sensor that is exposed to space radiation may be a significant source of random noise. Lastly, the availability and the lead time of the parts had to be considered. Although TOSHIBA's TCD sensor

presented in Table 3.2 has more desirable pixel parameters, it was not available during the time of the prototyping phase from any accessible distributors with unknown lead time. Thus the MLX75306 sensor by Melexis was chosen for this design.

The number of pixels and pixel pitch (the distance between the same side of two adjacent pixels) are important detector parameters. they are directly related to the resolution of the readout of the displacement of the pattern: the more pixels per unit length there are on the detector, the higher the resolution of the Sun Sensor. Using Equation 3.8 with $h = 2.3mm$ and distance set to 50 μm (corresponding to the pixel pitch of the MLX pixel array), the resolution of the Sun Sensor becomes 1.25°.

$$\theta_{res} = tan^{-1}(\frac{d_{pitch}}{h}) = tan^{-1}(\frac{50um}{2.3mm}) = 1.25^{\circ} \tag{3.8}$$

Due to the limited availability of the high resolution (low pixel pitch) photodiode arrays, the design of the Sun Sensor had to be altered to optimise the accuracy using the best available MLX chip.

3.2.3 Design parameters for manufacturing

MLX photodetector array was selected for the implementation on the two CubeSat missions to optimise for accuracy of the Sun Sensor. The physical characteristics of the linear optical array therefore became design constraints. Those constrained parameter differences are summarised in Table 3.3.

Similarly, constraints were imposed on the aperture mask due to manufacturing limitations. The material chosen for the aperture mask was a space grade Aluminum 6061. The only viable alternative to aluminium would be space grade non-outgassing plastic, for which the manufacturing turn-around time and cost were significantly higher at the time of the prototyping compared to aluminium machining. As such, the aperture mask design parameters were re-evaluated. The aperture mas parameters are summarised in Table 3.4.

Table 3.3: Photodiode array parameters

	Proposed design	**Implemented design**
Pixel pitch	8 μm	50 μm
Pixel size	5 μm	47 μm
Pixel count	256	142
Optical array length	2048 μm	7100 μm

The differences between the proposed aperture mask parameters and implemented mask were mainly driven by the smallest slit size that could be achieved. The chirped cosine basis for the mask pattern was abandoned, and instead the slit pattern was defined manually preserving the important properties: the centre slit has to be the largest slit, each pair of slits to the left and right of the centre have to be the same size, slits further away from the centre have to be smaller than the slits closer to the centre of the mask (see Figure 3.17). These properties ensure that each slit can be uniquely identified on the detector and therefore preserve the initial idea.

Table 3.4: Aperture mask parameters

	Proposed design	**Implemented design**
Slit pattern	chirped cosine	manually defined
Slit count	7	5
Mask Height	2.3 mm	3 mm
Mask length	2048 μm	7100 μm
Smallest slit	8 μm	500 μm
Resolution	0.2°	1.0°

As mentioned above, the resolution of the Sun Sensor is directly proportional to the height of the aperture mask (see Equation 3.1). Given the other 2 constraints: total height of a component must not be greater than 4 mm, and the smallest possible thickness of the aperture, which is 1 mm, the height of the mask was increased to the maximum possible 3 mm.

An updated sensor model with parameters presented above was created in MatLab, and the simulations were re-done to validate the updated design. The manufactured aperture mask is defined in Figure 3.17. Two sensor readouts with 20 dB SNR are depicted in Figure 3.18, which illustrates that having lower pixel density and larger pixel size, albeit causing lower resolution of the sensor, proves to be more resilient to noise. The RMS difference plots in Figure 3.19 show a similar pattern compared to the initially simulated model. There are distinct lines observed to the left and right of the global minimum. The slope of those lines was calculated to be 0.1727. With this model, 7100 samples of the noisy measurement were taken and the resulting distribution with $\pm 3\sigma$ values is presented in Figure 3.20. To compare this sensor model the ones simulated previously, the noise equivalent reading offset (O_r) defined in Equation 3.5 was calculated in Equation 3.9.

$$O_r(manufacturable) = \frac{0.4511}{0.1727} = 2.6123 \tag{3.9}$$

The noise equivalent offset value for the manufacturable sensor model fits between the single-slit and the chirped cosine-based model values, which is expected. However given the same signal to noise ration (20dB), the noise equivalent offset is significantly smaller than the pixel size and will not impact the readings of the sensor.

The detailed drawings containing all the dimensions of the manufactured masks for both of the implementations can be found in Appendix A.

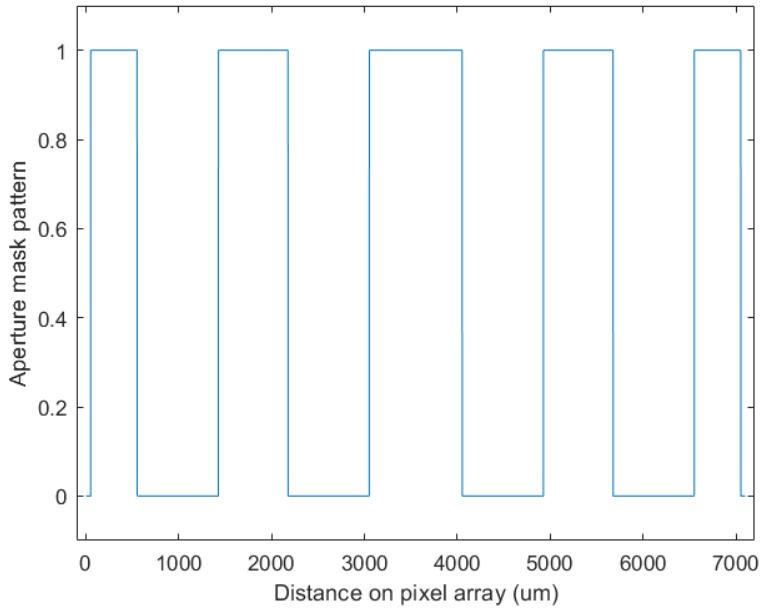

Figure 3.17: Definition of manufacturable aperture mask

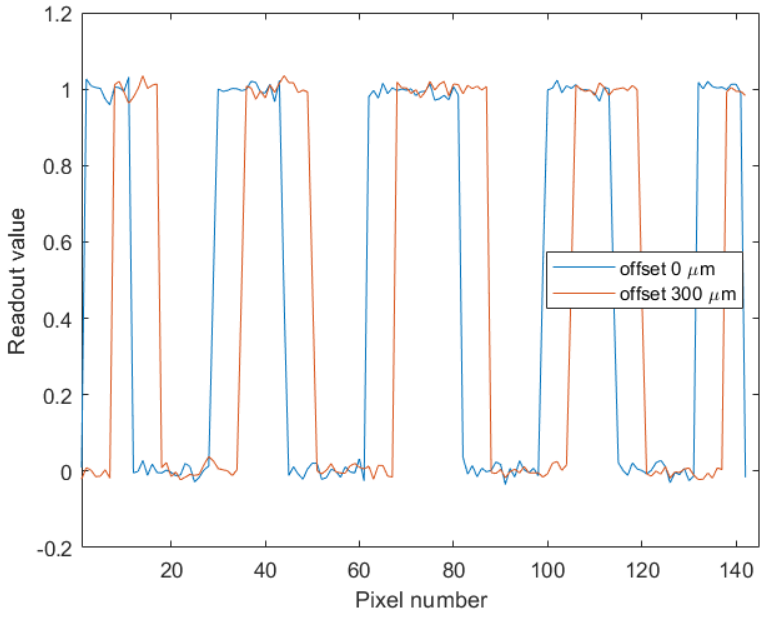

Figure 3.18: Pixel array readout plots for manufacturable mask pattern, centred at $0\mu m$ and $300\mu m$ offsets

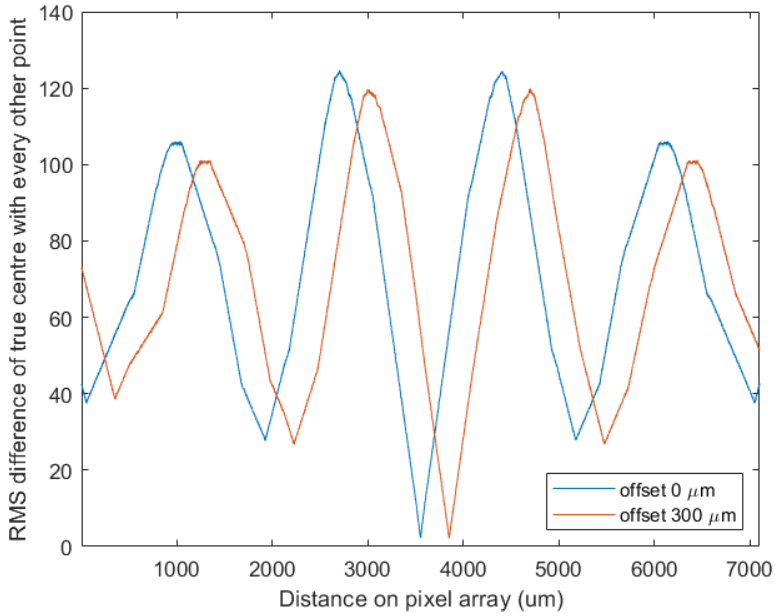

Figure 3.19: RMS difference of true centre of the projected mask pattern and all other possible locations on the sensor

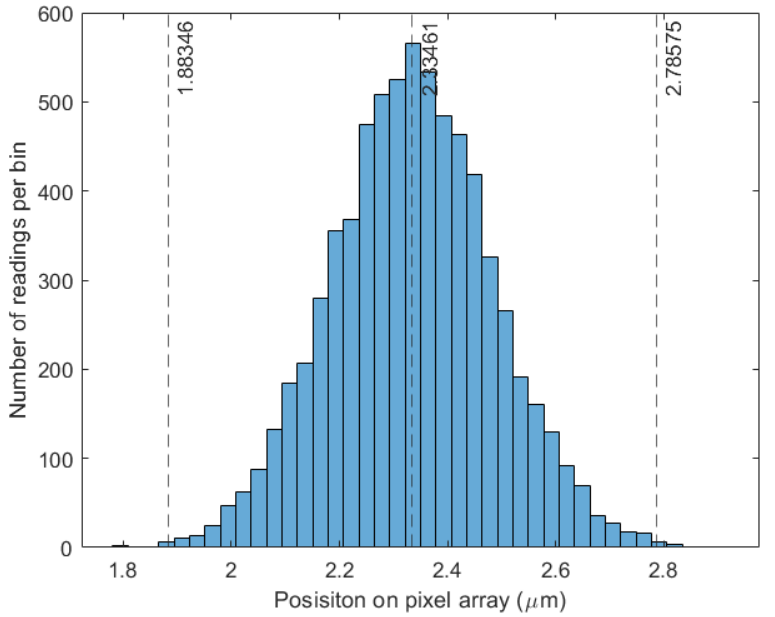

Figure 3.20: Noisy distribution of 7100 measurements given SNR of 20 dB

3.2.4 Readout Electronics Design

In designing readout electronics for the sensor, we started from the source of the signal, which in this case are photodetector chips. The signal originates from the photodiodes, which are analogue devices. Analogue signal needs to be converted to digital for any kind of processing and storage, thus an ADC is required. MLX photodetector chip has internal control and readout circuitry as well as high-speed ADC built in. The control logic of the chip is operated through Serial Programmable Interface (SPI), which is also used for data transfer.

Since the Sun Sensor is to be demonstrated in a nanosatellite payload, a set of requirements were imposed on the microcontroller. The most important microcontroller requirements are as follows: it has to be low power, small form factor, have an I2C interface and SPI interface for the Sun Sensor communication. SPI is one of the most common interfaces used in board-level digital communication, but it is not always included in small form-factor microcontrollers. Additionally, other important microcontroller characteristics were considered, such as the complexity, cost and availability of the development hardware, availability of the code libraries, memory size and programming interface.

For the solar cell technology demonstration payload implementation, Atmel ATtiny817 was selected, which features small form factor, low development cost, ultra-low power consumption, all required interfaces (I2C, SPI, USART) and libraries.

There are multiple modes of ADC operation available on MLX chip: 8-bit, 4-bit and 1-bit. These translate to quantization levels of the ADC conversion. In 8-bit readout mode, one pixel is represented by 8 bits, which means that one readout of one axis of the sensor will be $142 \times 8 = 1136$ bits. Since the proposed design is based on a binary pixel readout, 1-bit mode is used. This offloads the computing burden from the microcontroller as well as reduces the size of one readout from 1136 to 142 bits. Data size is an important consideration in satellite design, where the amount of data that can be transferred to the ground is very limited.

3.2.5 Data processing

The data received by the microcontroller is a digital 142-bit string per photodiode array. In this binary string zeros represent no light detected by the corresponding pixel, ones represent that light is detected by the corresponding pixel. This linear readout has to be converted to the angle of the Sun. Two fundamentally different approaches to data processing were considered for this conversion: computation and look-up table.

The computation based data processing approach requires little additional memory and relies on performing calculations that involve a simple digital filter or more sophisticated prediction based on a model. The most common method is the implementation of a model based filersuch as Extended Kalman Filter (EKF).

In a look-up table approach the processing is done in advance, and a table of values is stored in memory. Computational power required for this approach is minimal, however a significant memory capacity may be needed.

Given the constraints of the DESCENT mission, the data processing method is based on a look-up table approach, which will be implemented off the satellite. The look-up values are stored on the ground, and the raw data is stored and sent by the satellite. Since there are no constraints on the post-processing computation or memory, the RMS difference will be computed for each reading, similar to the operation done in the simulation and illustrated in Figure 3.19. This eliminates the requirement for additional memory and additional processing. This method is possible because the Sun Sensor is used for observation purposes only, and the angle information is not used by the satellite for attitude determination.

3.3 Integration with Solar Cell Anti-Reflection payload

3.3.1 Payload system level interconnection

As mentioned previously in Section 1.2, Solar Cell Anti-Reflection coating demonstration project is a stand-alone single PCB payload. The PCB houses all the components required for the operation of the payload. Since the PCB was designed specifically for integration into the DESCENT mission satellite, a set of constraints was imposed by the mission team. Among other important constraints, such as operation time, power consumption and data budget, the communication interface between the microcontroller of the payload and the On-Board Computer (OBC) of the satellite had to be SPI. This posed additional difficulty on the Sun Sensor integration in the payload: since the microcontroller of choice has only one SPI interface, the USART hardware had to be utilised for the communication with the Sun Sensor chips. USART interface is often used for development and debug of the microcontroller based embedded systems, which was the case with this payload. Thus the difficulty in integration was the absence of the debug interface, and the team had to rely on the programming interface of the microcontroller and a logic analyser for integration verification and debug.

3.3.2 Physical interface with the satellite

The payload PCB is slightly smaller than 10 by 10 cm square board with corner cutouts for mounting and a large 52.8 by 52.8 mm square cutout in the centre. The centre cutout was initially required for a GPS antenna, but as the mission requirements changed, the cutout was left for additional solar cells used for power production of the satellite. As shown in Figure 3.21, the payload PCB is mounted at the top face of the DESCENT mission 2U CubeSat and recessed back from the edge of the satellite such that the top plane of the Sun Sensor mask is flush with the edge of the satellite chassis.

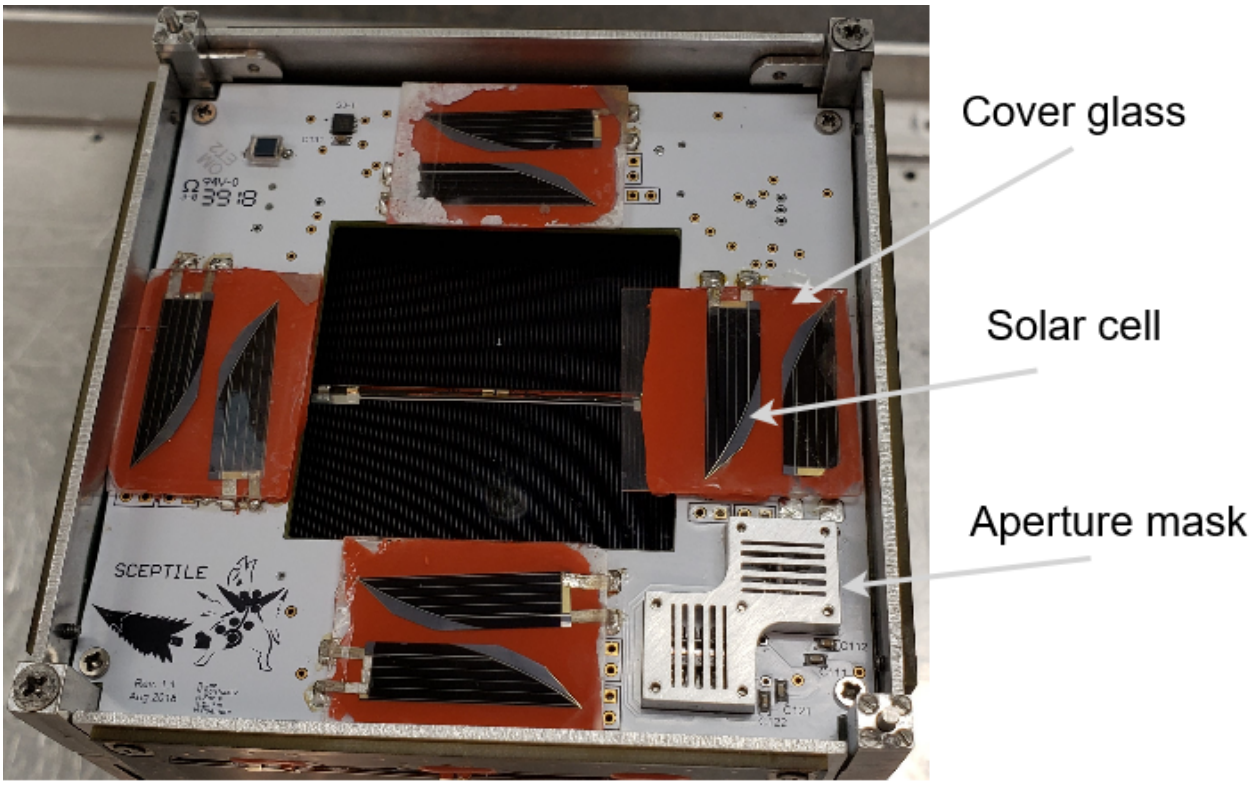

Figure 3.21: Solar Cell Anti-Reflection payload PCB, named "SCEPTILE" (Solar Cell Enhancing Panelglass Through Incident Light Experiment) fully populated and mounted on DESCENT satellite

3.3.3 Data and power interface with the satellite

As stated above, the communication interface between the satellite OBC and the Solar Cell payload microcontroller is SPI. A minimal SPI bus consists of one "master" and one "slave" device, which are connected by 4 wires: MOSI (Master Out, Slave In), MISO (Master In, Slave Out), SS (Slave Select) and SCK (Serial Clock) [41]. Additionally, the 3.3V and ground lines are provided from the OBC to the payload board, where the ground line is used for both power and signal ground. In this case, the payload microcontroller is a slave device, so these 6 lines are required and sufficient for power supply and data exchange. All 6 lines were combined in one connector specified by the mission team, which simplified the implementation and integration.

3.4 Integration with ManitobaSat-1 payload

In ManitobaSat-1 mission the Sun Sensor is a part of a payload and used as a reference, similar to Solar Cell payload in DESCENT mission. The payload design however is different and requires the Sun Sensor to be mounted on a separate PCB, which leads to all the SPI signals required for operation of 2 MLX chips combined in a larger connector. At the time of this writing the project is in early design phase, so requirements and design decisions may change. Current Sun Sensor PCB design snapshot and pictures of aperture mask prototype are presented in Figure 3.22 and Figures 3.23a, 3.23b respectively.

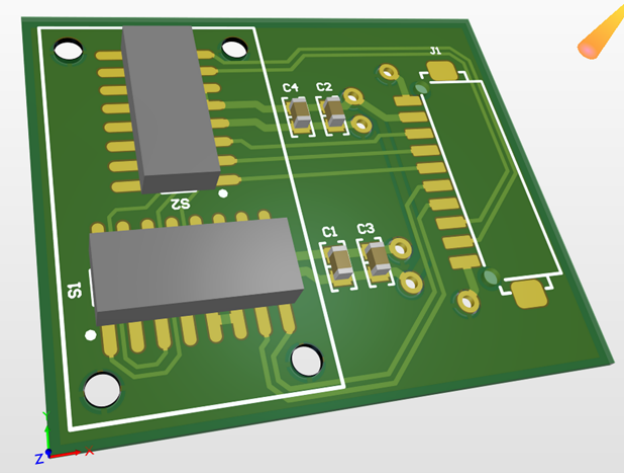

Figure 3.22: PCB design for ManitobaSat-1 Sun Sensor implementation

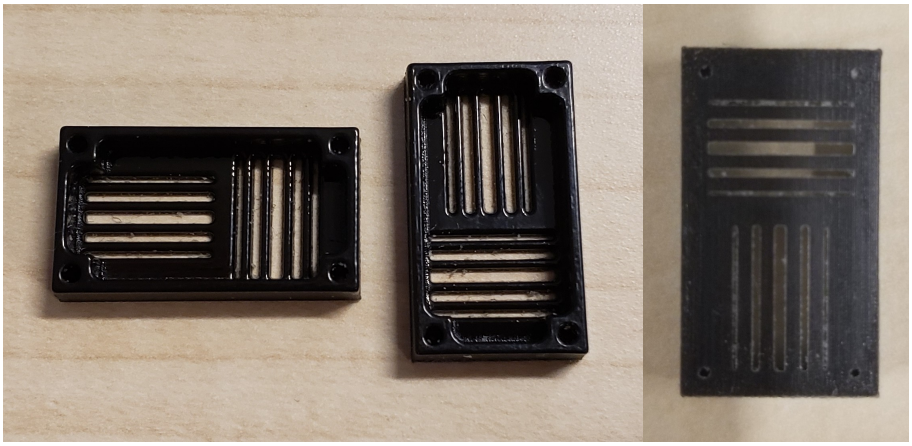

(a) Bottom side (b) Top side

Figure 3.23: Plastic prototype of Sun Sensor mask updated for ManitobaSat-1

Chapter 4

Characterization and Results

4.1 Laboratory setup for characterisation

The laboratory setup used for Sun Senor characterisation is presented in Figure 4.1. The main components of the setup are the rotation stage, board mount with Sun Sensor PCB, light source, and a computer connected to the Sun Sensor PCB (not shown on the diagram). The rotation stage consists of a stationary base and a platform. The platform is restricted to the single axis of rotation indicated by the arrows above the circular platform on the diagram. The platform has a mark aligned to the centre of the mount, while the base has index marks indicating the rotation angle. The board mount was fashioned from a tablet stand and allows for nearly vertical mounting of the PCB on the rotation stage. The light source used is a portable work light with 300 watt bulb. The PCB was connected to a computer, which recorded the measurements from the photodetector arrays.

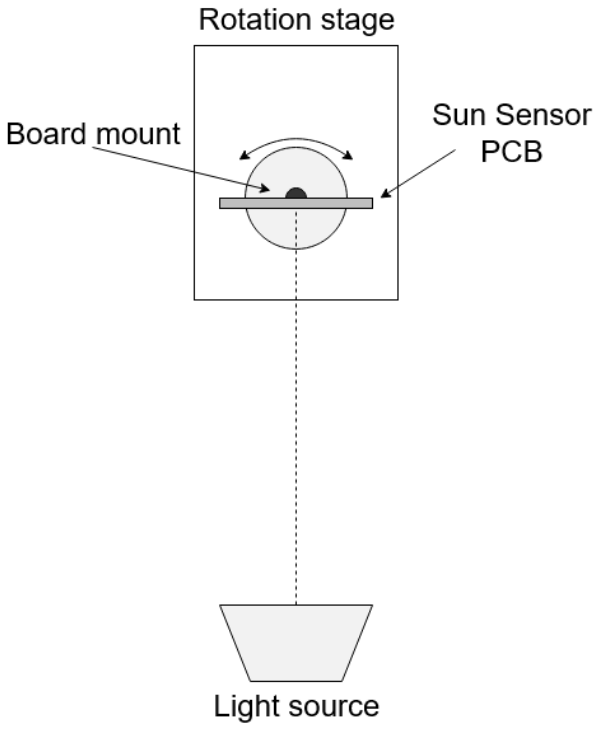

Figure 4.1: Diagram of laboratory setup for Sun Sensor characterisation (top view)

4.2 Characterisation procedure

The PCB with the Sun Sensor was mounted on the rotational platform such that the centre of horizontally oriented photodiode array of the Sun Sensor was aligned with the centre of the axis of rotation. The horizontal orientation of the PCB was verified with a level. The light source was placed 2 metres away from the rotational stage. The platform was set to normal incidence angle (0 degrees) and 10 consecutive readings were taken and recorded. The angle was then changed in increments of 0.5 degrees and 10 measurements were taken for each position until 30 degrees were reached. The same procedure was repeated for the other, negative, side until -30 degrees were reached. The whole procedure was carried out for the second photodiode array, corresponding to the second axis by rotating the PCB 90 degrees and re-mounting it on the platform.

4.3 Results and discussion

As shown on the figures below, the Sun Sensor was characterised in the range of −30 to +30 of incident light for each photodetector chip, corresponding to X and Y axes. Although the field of view was estimated to be approximately ±50 degrees, the theoretical estimate did not take the finite thickness of the aperture into account. The tapering of each region corresponding to a slit can be especially well seen in Figure 4.3, where the rightmost slit nearly diminishes at −30 degrees. This does not mean that the sensor will not operate past −30 degrees, of course. The other, wider, slits are still detected, and the pattern is still unique. This rather illustrates that the design can benefit from the implementation of the mask that minimises the thickness of the aperture. The plots have artifacts, the readings that are far from expected, which is especially well seen in Figure 4.2, where readings corresponding to four different angles appear to be out of place. This is likely due to the internal reflections of light off the aperture mask, since the surface of the machined part made out of aluminium is quite glossy. Alternatively, the artifacts may be a concequence of some data corruption, which would have been difficult to notice during the characterisation of the sensor. On both of the figures depicting the readouts from the detector corresponding to the X axis, a dead pixel (number 130) can be seen. A defect like that, provided only one pixel is not functional, will impact the accuracy marginally, if at all. Figure 4.3 has the least amount of artifacts and appears to be the closest of all to expectations. The diagrams show that lines corresponding to readings of one degree apart from each other have very few of or do not have any overlapping grey pixels. This shows that the accuracy of the sensor given raw, uncalibrated data is 1 degree. With a few exceptions, the majority of the consecutive readings have at least a few pixels different or grey (some percentage of samples are different). This shows the potential for further accuracy improvement. Assuming that a rotation table calibrated to higher accuracy than 0.5° is used, it is possible to calibrate the implemented Sun Sensor to be accurate to 0.5°, which may be further improved by signal processing.

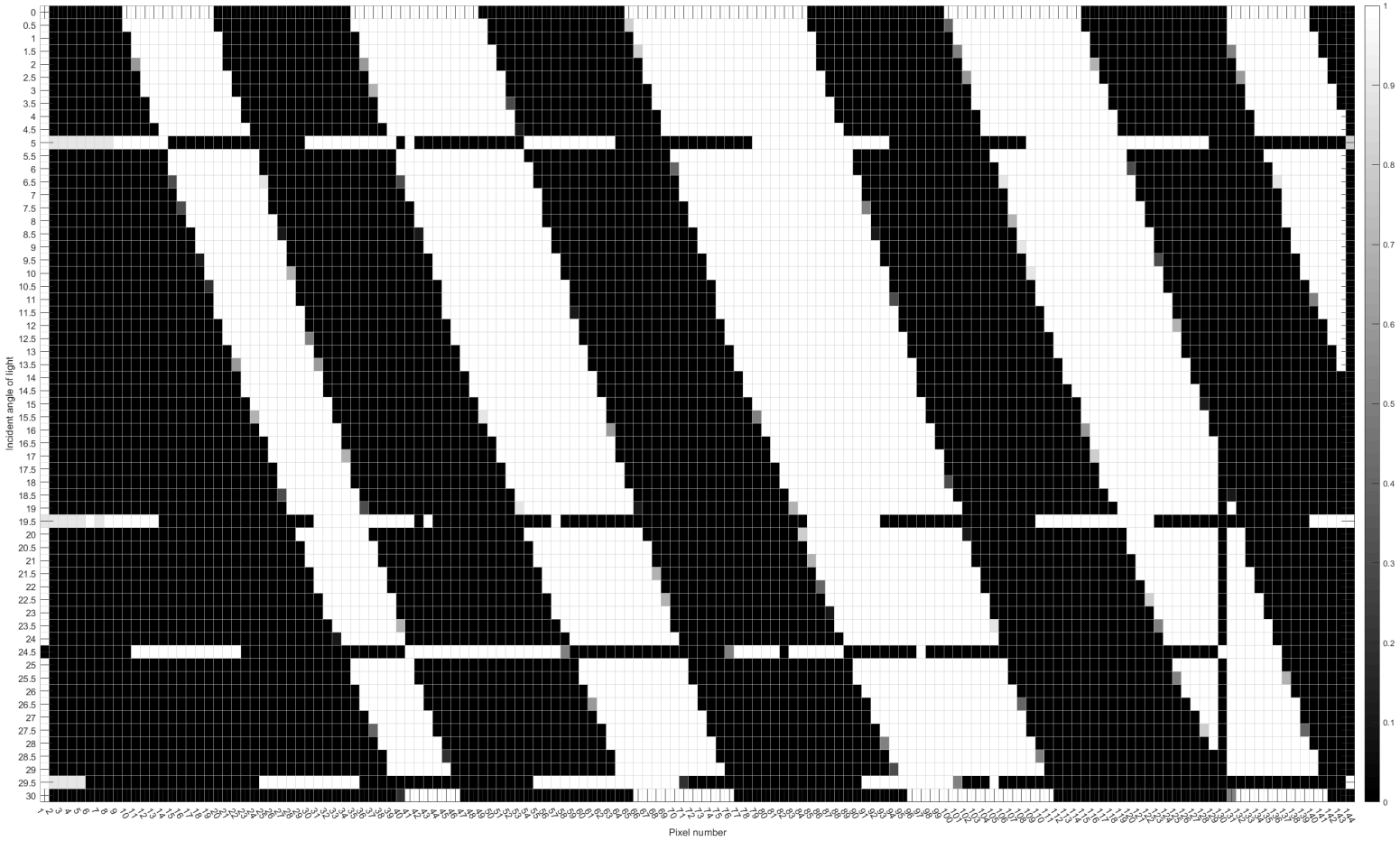

Figure 4.2: X axis detector pixel map of positive angles (rotation to the right)

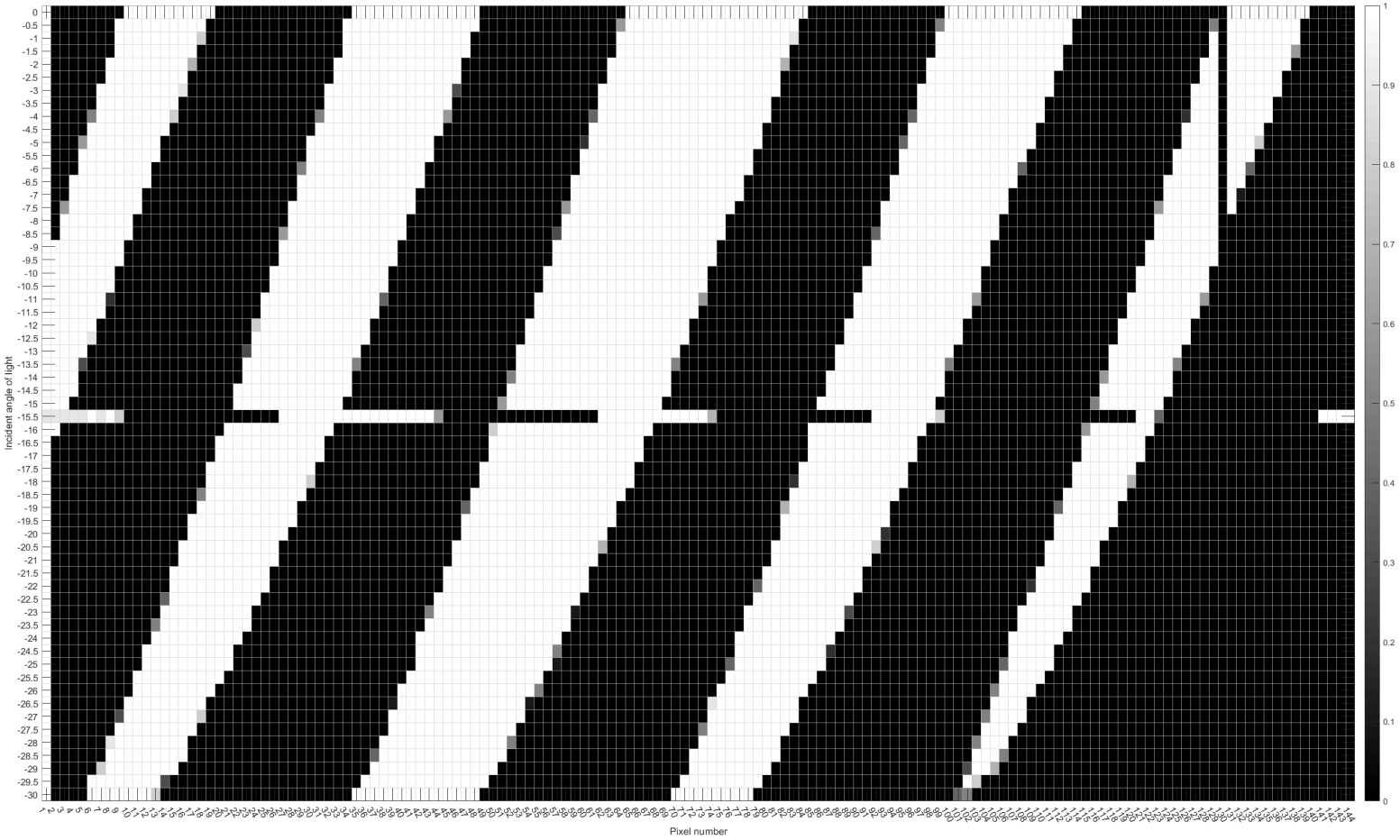

Figure 4.3: X axis detector pixel map of negative angles (rotation to the left)

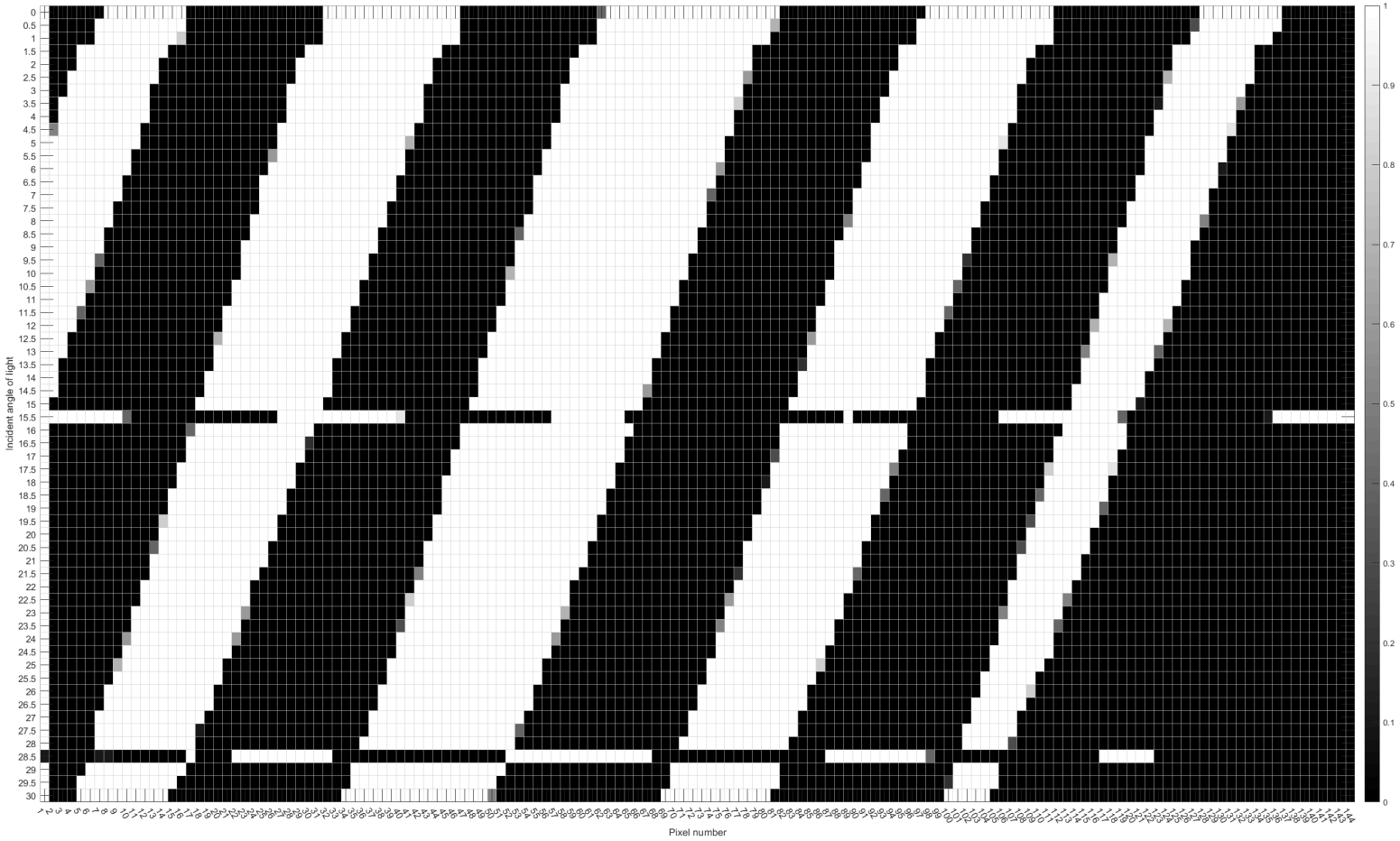

Figure 4.4: Y axis detector pixel map of positive angles (rotation to the right)

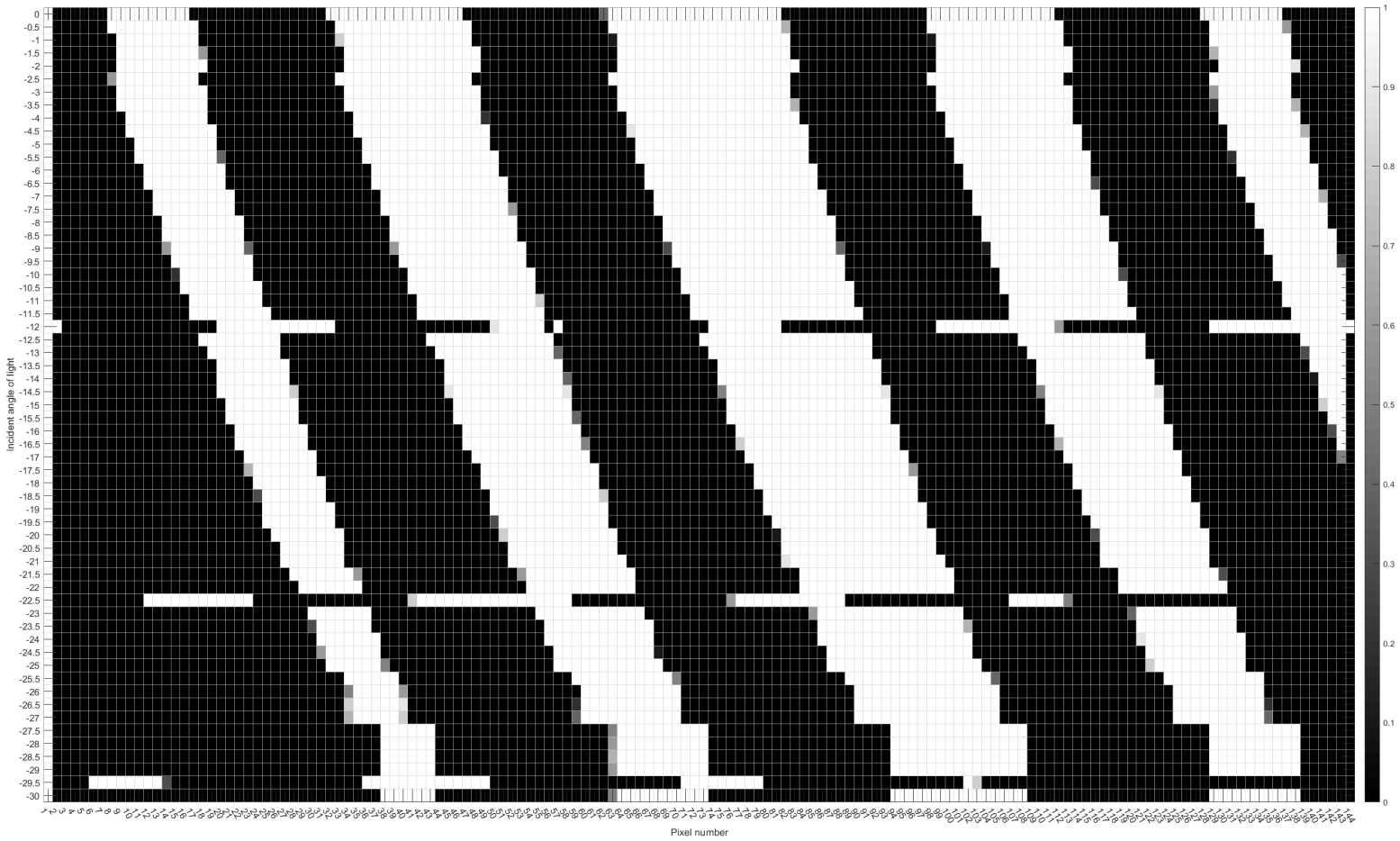

Figure 4.5: Y axis detector pixel map of negative angles (rotation to the left)

Chapter 5

Final remarks

A new digital Sun Sensor design has been proposed, formulated, implemented and validated in laboratory environment. Thus the work done and results presented in this thesis have taken the proposed concept from Technology Readiness Level 1 (TRL 1) to TRL 4 [42]. At the time of writing, the DESCENT mission satellite is fully assembled, tested and ready for launch, which is planned in January 2020. The satellite component and system validation steps have taken the Sun Sensor from TRL 4 to TRL 6. The launch, assuming successful operation of the mission, will bring the technology readiness level from TRL 6 to TRL 7. Thus the work presented in this thesis delivers another candidate to space-qualified products of Canadian space industry through flight heritage on a CubeSat mission.

There are several areas where the Sun Sensor can be improved. The sensor characterisation can be improved by calibrating the rotation table or using a calibrated, electronically controlled rotation table with accuracy higher than the predicted best calibrated accuracy of the sensor. Additionally, the characterisation and testing of the field of view would benefit from further exploration. The accuracy is expected to decrease at higher angles of light, which should be mitigated by the presence of multiple slits. Both the accuracy at higher angles and the real detection angle limit improvements can be explored by manufacturing the aperture mask with thinner aperture. Further accuracy improvements are expected through the

implementation a model-based signal processing algorithm or filter, such as Extended Kalman Filter. Additionally, accuracy may be improved by going away from the binary readout mode of the ADC, since the readout value of the edge pixels will then be proportional to the intensity of light, potentially leading to sub-pixel accuracy on its own, without any other improvements mentioned above. The light reflections off of the aperture mask can be mitigated or potentially eliminated by anodizing the aluminium mask in matte black or using black space grade plastic.

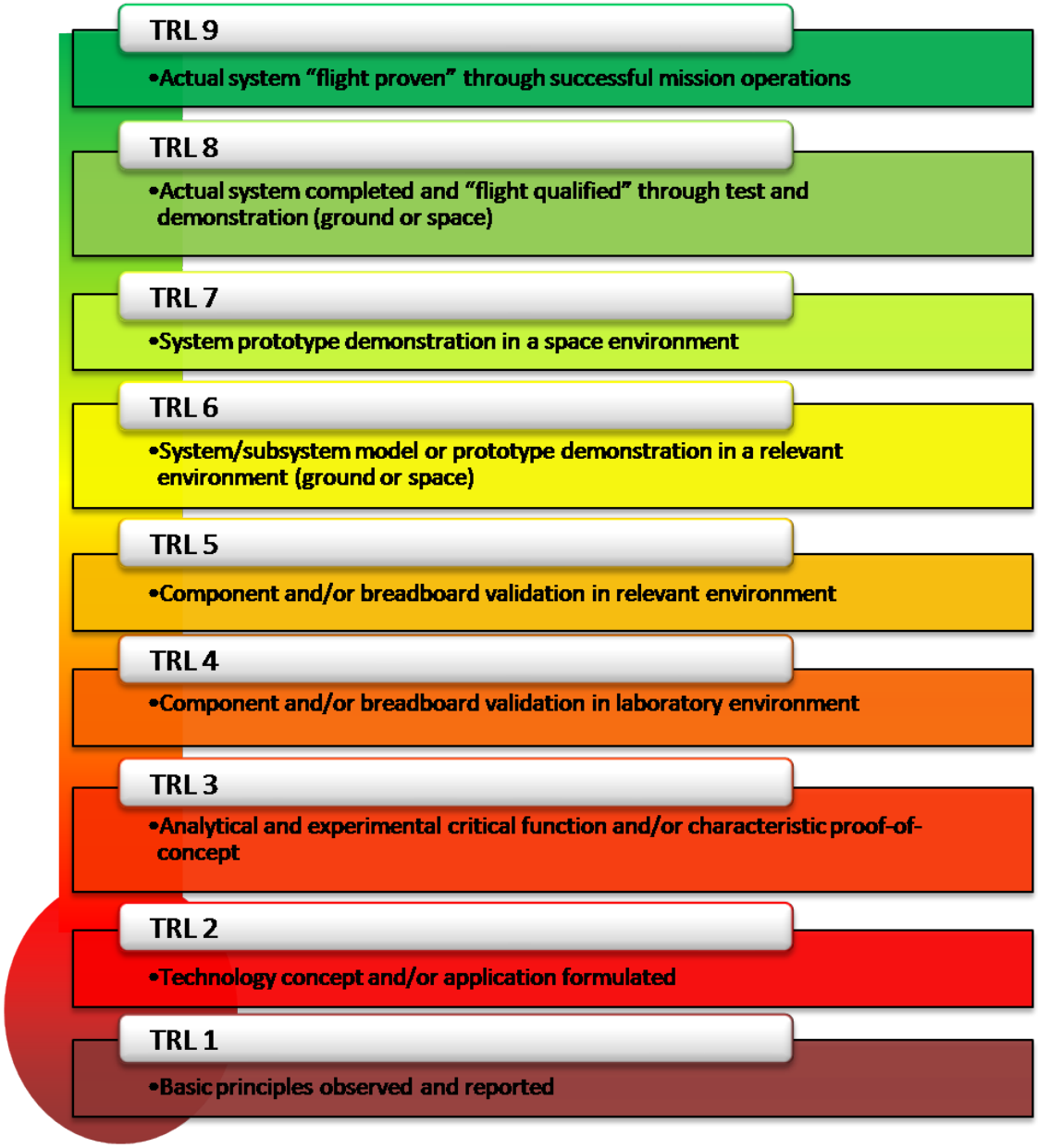

Figure 5.1: Technology Readiness Level (TRL) descriptions.

Source: Image downloaded from `https://www.nasa.gov/directorates/heo/scan/engineering/technology/txt_accordion1.html`

References

[1] Heiner Lasi et al. "Industry 4.0". In: *Business & Information Systems Engineering* 6.4 (Aug. 2014), pp. 239–242. ISSN: 1867-0202. DOI: 10.1007/s12599-014-0334-4. URL: https://doi.org/10.1007/s12599-014-0334-4.

[2] Paul S. Peercy. "The drive to miniaturization". In: *Nature* 406 (2000), pp. 1023–1026. ISSN: 1476-4687. DOI: https://doi.org/10.1038/35023223.

[3] Wen H. Ko. "Trends and frontiers of MEMS". In: *Sensors and Actuators A: Physical* 136.1 (2007). 25th Anniversary of Sensors and Actuators A: Physical, pp. 62–67. ISSN: 0924-4247. DOI: https://doi.org/10.1016/j.sna.2007.02.001. URL: http://www.sciencedirect.com/science/article/pii/S0924424707000489.

[4] Gottfried Konecny. "Small Satellites - a tool for Earth Observation?" In: (2004).

[5] Erik Kulu. *Nanosats Database*. https://www.nanosats.eu/. Accessed: 2019-07-01.

[6] Edificio Tecnológico Aeroespacial. *A Basic Guide to Nanosatellites*. https://alen.space/basic-guide-nanosatellites/. Accessed: 2019-07-13.

[7] CubeSatShop.com. *One-stop webshop for CubeSats & Nanosats*. Accessed: 2019-07-14.

[8] Armen Poghosyan and Alessandro Golkar. "CubeSat evolution: Analyzing CubeSat capabilities for conducting science missions". In: *Progress in Aerospace Sciences* 88 (2017), pp. 59–83. ISSN: 0376-0421. DOI: https://doi.org/10.1016/j.paerosci.

2016.11.002. URL: http://www.sciencedirect.com/science/article/pii/S0376042116300951.

[9] Daniel Selva and David Krejci. "A survey and assessment of the capabilities of Cubesats for Earth observation". In: *Acta Astronautica* 74 (2012), pp. 50–68. ISSN: 0094-5765. DOI: https://doi.org/10.1016/j.actaastro.2011.12.014. URL: http://www.sciencedirect.com/science/article/pii/S0094576511003742.

[10] J. Bouwmeester and J. Guo. "Survey of worldwide pico- and nanosatellite missions, distributions and subsystem technology". In: *Acta Astronautica* 67.7 (2010), pp. 854–862. ISSN: 0094-5765. DOI: https://doi.org/10.1016/j.actaastro.2010.06.004. URL: http://www.sciencedirect.com/science/article/pii/S0094576510001955.

[11] Franco Davoli et al. "Small satellites and CubeSats: Survey of structures, architectures, and protocols". In: *International Journal of Satellite Communications and Networking* 37.4 (2019), pp. 343–359. DOI: 10.1002/sat.1277. eprint: https://onlinelibrary.wiley.com/doi/pdf/10.1002/sat.1277. URL: https://onlinelibrary.wiley.com/doi/abs/10.1002/sat.1277.

[12] CubeSat shop. *NSS Fine Sun Sensor*. URL: https://www.cubesatshop.com/product/digital-fine-sun-sensor/ (visited on 07/05/2019).

[13] NewSpace Systems. *NewSpace Sun Sensor*. URL: https://www.cubesatshop.com/wp-content/uploads/2016/06/NewSpace-Sun-Sensor_7b.pdf (visited on 07/05/2019).

[14] Lens Research & Development. *Product Specification BiSon64-ET - Acada Landing Product*. URL: https://lens-rnd.com/download/product-specification-bison64-et/ (visited on 07/05/2019).

[15] Solar MEMS Technologies S.L. *nanoSSOC-A60 Sun Sensor for Nano-Satellites, Analog Interface*. URL: https://www.cubesatshop.com/wp-content/uploads/2016/06/nanoSSOC-A60-Technical-Specifications.pdf (visited on 07/05/2019).

[16] Solar MEMS Technologies S.L. *nanoSSOC-D60 Sun Sensor for Nano-Satellitesm, Digital Interface*. URL: https://www.cubesatshop.com/wp-content/uploads/2016/06/nanoSSOC-D60-Technical-Specifications.pdf (visited on 07/05/2019).

[17] CubeSat shop. *NSS CubeSat Sun Sensor*. URL: https://www.cubesatshop.com/product/nss-cubesat-sun-sensor/ (visited on 07/05/2019).

[18] Anwar Ali et al. "Innovative power management, attitude determination and control tile for CubeSat standard NanoSatellites". In: *Acta Astronautica* 96 (2014), pp. 116–127. ISSN: 0094-5765. DOI: https://doi.org/10.1016/j.actaastro.2013.11.013. URL: http://www.sciencedirect.com/science/article/pii/S0094576513004165.

[19] Vidushi Jain et al. "Practical Implementation of Test-As-You-Fly for the DESCENT CubeSat Mission". In: *2018 SpaceOps Conference* (). DOI: 10.2514/6.2018-2691. eprint: https://arc.aiaa.org/doi/pdf/10.2514/6.2018-2691. URL: https://arc.aiaa.org/doi/abs/10.2514/6.2018-2691.

[20] *DESCENT*. URL: http://www.yorku.ca/edtsat/ (visited on 07/17/2019).

[21] *MBSat-1*. URL: https://sites.google.com/site/manitobasat1/home (visited on 12/05/2019).

[22] Hugh Podmore. "Subwavelength Antireflection for Space Applications". MA thesis. Toronto, Ontario, Canada: York University, 2015.

[23] ManitobaSat-1 design team. *ManitobaSAT-1 Canadian CubeSat Proposal*.

[24] Kristian Svartveit. "Attitude determination of the NCUBE satellite". In: *NTNU, June* (2003). URL: http://folk.ntnu.no/tomgra/Diplomer/Svartveit.pdf.

[25] Carl C Liebe et al. "Active pixel sensor (APS) based star tracker". In: *1998 IEEE Aerospace Conference Proceedings (Cat. No. 98TH8339)*. Vol. 1. IEEE. 1998, pp. 119–127. URL: https://ieeexplore.ieee.org/abstract/document/686811.

[26] Mario H Acuna. "Space-based magnetometers". In: *Review of scientific instruments* 73.11 (2002), pp. 3717–3736. URL: https://aip.scitation.org/doi/abs/10.1063/1.1510570.

[27] Hongwei Qu et al. "High-resolution integrated micro-gyroscope for space applications". In: *41st space congress*. 2004, pp. 75–82. URL: https://www.researchgate.net/profile/Huikai_Xie/publication/237135654_High-resolution_Integrated_Micro-gyroscope_for_Space_Applications/links/02e7e52c80b9f08df2000000/High-resolution-Integrated-Micro-gyroscope-for-Space-Applications.pdf.

[28] Carl C Liebe et al. "Three-axis sun sensor for attitude determination". In: *IEEE Aerospace and Electronic Systems Magazine* 31.6 (2016), pp. 6–11. URL: https://ieeexplore.ieee.org/abstract/document/7501228.

[29] Erik Babcock. "CubeSat attitude determination via Kalman filtering of magnetometer and solar cell data". In: *Small Satellite Conference* (2011).

[30] Alexander Kocian et al. "Analog solar sensor as payload in edusat satellite". In: Mar. 2010. DOI: 10.1109/AERO.2010.5446915.

[31] L. Farian, P. Hafliger, and J. A. Lenero-Bardallo. "Miniaturized Sun sensor with in-pixel processing for Attitude Determination of micro space probes". In: *2015 International Conference on Event-based Control, Communication, and Signal Processing (EBCCSP)*. June 2015, pp. 1–6. DOI: 10.1109/EBCCSP.2015.7300688. URL: https://ieeexplore.ieee.org/abstract/document/7300688.

[32] L. Farian, P. Hafliger, and J. A. Lenero-Bardallo. "A Miniaturized Two-Axis Ultra Low Latency and Low-Power Sun Sensor for Attitude Determination of Micro Space Probes". In: *IEEE Transactions on Circuits and Systems I: Regular Papers* 65.5 (May 2018), pp. 1543–1554. DOI: 10.1109/TCSI.2017.2763990. URL: https://ieeexplore.ieee.org/abstract/document/8094260.

[33] Shawn Allgeier, Matt Mahin, and Norman Fitz-Coy. "Design and analysis of a coarse sun sensor for pico-satellites". In: *AIAA Infotech@ Aerospace Conference and AIAA Unmanned... Unlimited Conference*. 2009, p. 1837. URL: https://arc.aiaa.org/doi/abs/10.2514/6.2009-1837.

[34] John C. Springmann and James W. Cutler. "Flight results of a low-cost attitude determination system". In: *Acta Astronautica* 99 (2014), pp. 201–214. ISSN: 0094-5765. DOI: https://doi.org/10.1016/j.actaastro.2014.02.026. URL: http://www.sciencedirect.com/science/article/pii/S0094576514000836.

[35] Martin Nygren, R Birkeland, and JT Gravdahl. "Using solar panels as sun sensors on ntnu test satellite". In: *Norwegian University of Science and Technology, Norwegian University of Science and Technology* (2012). URL: http://citeseerx.ist.psu.edu/viewdoc/download?doi=10.1.1.462.6129&rep=rep1&type=pdf.

[36] Mohamed Zahran and Mohamed Aly. "A solar cell based coarse sun sensor for a small leo satellite attitude determination". In: *Journal of Power Electronics* 9.4 (2009), pp. 631–642. URL: https://www.researchgate.net/profile/Mohamed_Zahran5/publication/238734661_A_Solar_Cell_Based_Coarse_Sun_Sensor_for_a_Small_LEO_Satellite_Attitude_Determination/links/02e7e52a5eac8452e5000000/A-Solar-Cell-Based-Coarse-Sun-Sensor-for-a-Small-LEO-Satellite-Attitude-Determination.pdf.

[37] I. Maqsood and T. Akram. "Development of a low cost sun sensor using quadphotodiode". In: *IEEE/ION Position, Location and Navigation Symposium*. May 2010, pp. 639–644. DOI: 10.1109/PLANS.2010.5507186. URL: https://ieeexplore.ieee.org/abstract/document/5507186.

[38] Feifan Chen and Jing Feng. "Analogue sun sensor based on the optical nonlinear compensation measuring principle". In: *Measurement Science and Technology* 18.7

(June 2007), pp. 2111–2115. DOI: 10.1088/0957-0233/18/7/042. URL: https://iopscience.iop.org/article/10.1088/0957-0233/18/7/042/meta.

[39] Fei Xing et al. "A novel active pixels sensor (APS) based sun sensor based on a feature extraction and image correlation (FEIC) technique". In: *Measurement Science and Technology* 19.12 (Oct. 2008), p. 125203. DOI: 10.1088/0957-0233/19/12/125203. URL: https://iopscience.iop.org/article/10.1088/0957-0233/19/12/125203/meta.

[40] Jaroslav Chum and Jaroslav Vojta. "Wide angle digital slit sun sensor using CCD linear array". In: *International Conference on Space Optics — ICSO 2000*. Ed. by Georges Otrio. Vol. 10569. International Society for Optics and Photonics. SPIE, 2017, pp. 690–698. DOI: 10.1117/12.2307889. URL: https://doi.org/10.1117/12.2307889.

[41] SPI Block Guide. "V03. 06.: Motorola". In: *Inc., February* (2003). URL: https://web.archive.org/web/20150413003534/http://www.ee.nmt.edu/~teare/ee308l/datasheets/S12SPIV3.pdf.

[42] NASA. *Technology Readiness Level*. 2017. URL: www.nasa.gov/directorates/heo/scan/engineering/technology/txt_accordion1.html (visited on 12/02/2019).

Appendix: Sun Senor mask drawings

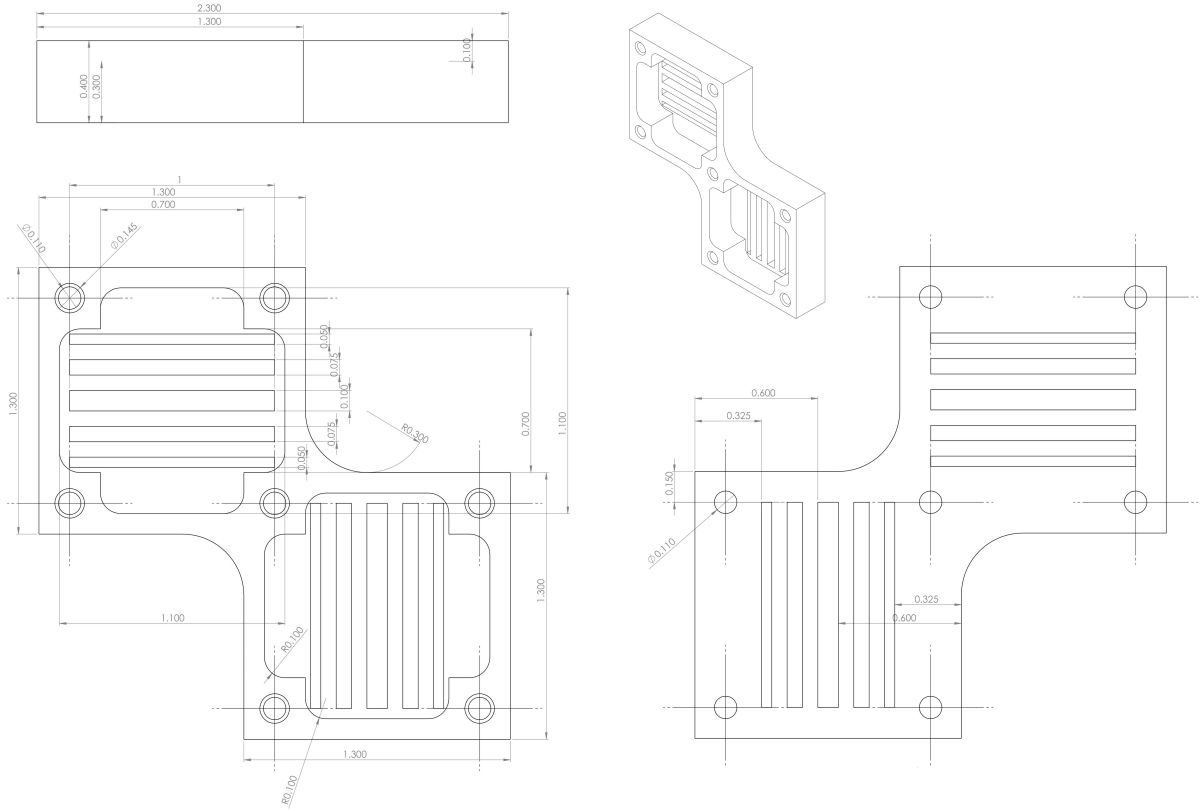

DESCENT mission Sun sensor mask drawing (version 4)

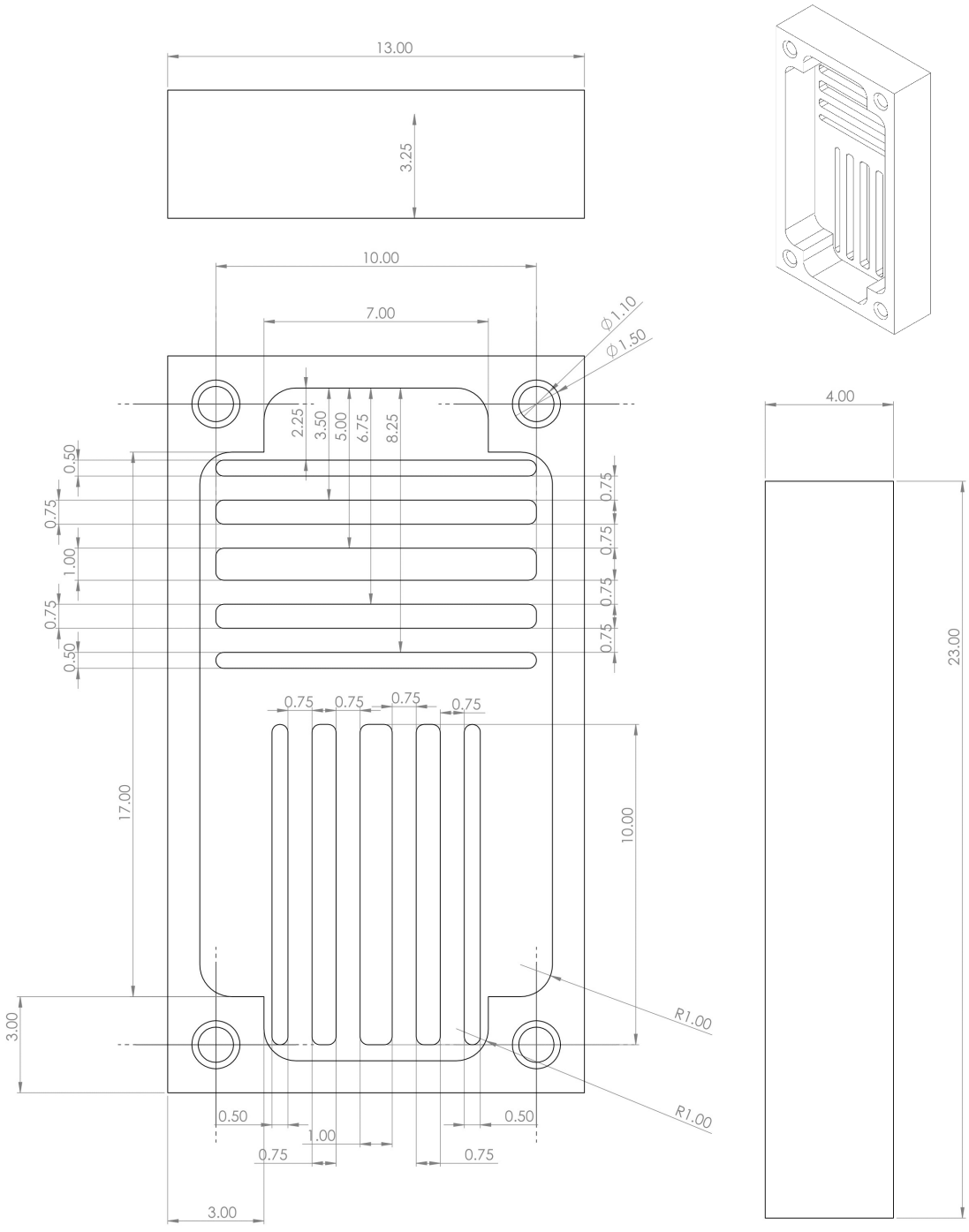

ManitobaSat-1 mission Sun sensor mask drawing (version 5)